geosciences

Review

Squeezing Data from a Rock: Machine Learning for Martian Science

Timothy Paul Nagle-McNaughton [1,*], Louis Anthony Scuderi [1] and Nicholas Erickson [2]

1 Department of Earth and Planetary Science, The University of New Mexico, Albuquerque, NM 87131, USA; tree@unm.edu
2 Cloud to Street, 147 Prince St., New York, NY 11201, USA; cole.erickson@gmail.com
* Correspondence: timnaglemcnaughton@unm.edu

Abstract: Data analysis methods have scarcely kept pace with the rapid increase in Earth observations, spurring the development of novel algorithms, storage methods, and computational techniques. For scientists interested in Mars, the problem is always the same: there is simultaneously never enough of the right data and an overwhelming amount of data in total. Finding sufficient data needles in a haystack to test a hypothesis requires hours of manual data screening, and more needles and hay are added constantly. To date, the vast majority of Martian research has been focused on either one-off local/regional studies or on hugely time-consuming manual global studies. Machine learning in its numerous forms can be helpful for future such work. Machine learning has the potential to help map and classify a large variety of both features and properties on the surface of Mars and to aid in the planning and execution of future missions. Here, we outline the current extent of machine learning as applied to Mars, summarize why machine learning should be an important tool for planetary geomorphology in particular, and suggest numerous research avenues and funding priorities for future efforts. We conclude that: (1) moving toward methods that require less human input (i.e., self- or semi-supervised) is an important paradigm shift for Martian applications, (2) new robust methods using generative adversarial networks to generate synthetic high-resolution digital terrain models represent an exciting new avenue for Martian geomorphologists, (3) more effort and money must be directed toward developing standardized datasets and benchmark tests, and (4) the community needs a large-scale, generalized, and programmatically accessible geographic information system (GIS).

Keywords: Mars; machine learning; remote sensing; geomorphology; surface processes; planetary science

Citation: Nagle-McNaughton, T.P.; Scuderi, L.A.; Erickson, N. Squeezing Data from a Rock: Machine Learning for Martian Science. *Geosciences* **2022**, *12*, 248. https://doi.org/10.3390/geosciences12060248

Academic Editors: Alberto G. Fairén and Jesus Martinez-Frias

Received: 24 April 2022
Accepted: 6 June 2022
Published: 15 June 2022

1. Introduction

The recent increase in the development and deployment of machine learning (ML) for Earth observation has led to a wealth of new data and insights about our planet. These ML methods—enabled by more numerous and advanced satellites, increasingly sophisticated detection algorithms, and faster computation resources—are required since the expansion of data collected on Earth has rapidly outpaced the speed of manual analysis. As more and more data are collected, automation of time-consuming tasks by algorithms has become more important. Examples of these tasks include sensor calibration, image preprocessing, image segmentation, feature extraction, and classification of features and land cover.

Given the difficulty and expense of imaging Mars, there has not been the same influx of new instruments nor the return of data at rates and quantities equal to those from Earth-orbiting satellites. That said, there are currently more instruments collecting Martian data than there have ever been in the past: of the 18 successful orbital missions around Mars, eight are currently active, and of the seven successful lander missions on Mars, three are still active. Furthermore, there are already large archives of Martian imagery data available in the National Aeronautics and Space Administration's (NASA's) Planetary Data System (PDS) [1,2] and the European Space Agency's (ESA's) Planetary Science Archive (PSA) [3,4]. While the quantity of the data is smaller, the Mars science community is relatively small given the lack of corporate profit incentive to analyze Mars data, leading to an outpacing of manual analysis.

Several interesting and unique problems make the application of ML approaches to Martian data an area of potentially significant value. The autonomy of rovers on the Martian surface has long been an area of great interest due to (1) the long time delay between signals and instructions sent between Earth and Mars, (2) an asynchronistic overlap between the Earth and Mars days, and (3) the desire for rovers to make mission progress even when they are not executing specific instructions from Earth. In recent years, robotic autonomy has progressed from overcoming driving navigation problems to including tasks such as selecting sample targets [5–7] and even guiding landers to safe landing areas [8–15]. While efficiently managing rover time is one area of focus, rover missions to Mars are expensive and require years of planning, but can only study an infinitesimally small fraction of the Martian surface. With these inherent limitations, there is a strong incentive to both (1) use satellite data to effectively identify locations of the greatest interest and suitability for a rover mission, and (2) use remote sensing wherever possible to learn as much as possible without the need for in situ rover observations [16,17]. Thus, the need to leverage the archives of Martian observations is an increasingly important focus for Mars researchers, and planetary scientists more broadly: "Mars is a uniquely enabling study target for investigations of surface processes active on other planetary bodies—both for extending terrestrial based process models and, in some areas, for serving as a superior comparative planetology basis over Earth" [16]. This is especially important given the range of major outstanding questions that ML could potentially help answer [18,19].

Scope and Audience

We do not intend this paper to be a review of methods currently employed in Earth observation as there are already many excellent review papers that cover that topic [20–36]. Similarly, rover navigation will not be our focus here as the topic has been covered elsewhere [37–54]. Instead, we aim to provide a novel summary of the state of ML for Mars observation, and to help further Martian research by highlighting under-explored domains. To that end, we set out with four goals: (1) to help to connect the planetary science and ML communities, (2) to collect and categorize the current state-of-the-art research methods used in Martian studies, (3) to offer a perspective on the future of automated methods, and (4) to identify opportunities for further studies. Our intended audience is twofold: (1) planetary scientists seeking to explore how ML could improve their research, or make their experiments more efficient, and (2) ML experts who can help collect, organize, and analyze data for Martian studies.

For the purposes of this paper, we use a broad definition of ML: a subdomain of artificial intelligence in which algorithms self-optimize to improve their results. While there are many further subdomains within the discipline, such as deep learning, active learning, computer vision, and natural language processing, here, we will use the umbrella term ML to capture the full breadth of these approaches as applied to Mars research.

2. Machine Learning Studies on Mars

Generally, there are two methods for structuring a description of different types of ML: learning-focused frameworks that center on the functioning of the algorithm in question, or task-focused frameworks that focus on the algorithm's product rather than its method. For this paper, we have opted to use the learning-focused framework, with subsections for each type of task which contain research in that domain.

2.1. Supervised Learning

Supervised learning requires labeled data as both the input and target when fed into the ML algorithm; algorithms are fit to these data, and a trained model predicts targets for unknown inputs [55–59]. The two most common applications of supervised learning are classification and regression problems. In classification problems, the input data are mapped onto pre-defined categories, while in regression problems, the input data are mapped to numerical outputs. For example, a supervised classification network could be trained on images of cats and dogs, with each of the images having a corresponding label indicating whether the image contains a cat or a dog. The network could then be given an unlabeled image of a cat and—if trained well—identify that the image contains a cat. In contrast, a supervised regression network could be trained on several years worth of daily weather data. The model could then predict the temperature for any given day of the year.

2.1.1. Classification

Transfer Learning

Transfer learning is a popular method for decreasing the time required to train a model on a new set of data [60–64]. Transfer learning is simply the application of pre-learned weights or filters to a new dataset. In essence, a model trained for one task is applied to another, with the assumption that the two tasks are appropriately related. In image classification, this is intuitive: object recognition across domains typically requires pattern extraction, edge detection, and other standard image-processing steps. A model trained to recognize cats in images could quickly be adapted to recognize dogs without having to reset the model's weights and begin training from scratch. Many complex models have been published that have been pre-trained on large datasets of text or images [65–73]. These off-the-shelf models allow researchers to take advantage of the complexity and depth of the models while reducing the time required to develop and train a model. The application of transfer learning is limited in Martian research, but its use is highlighted in the following sections.

Classification Applications on Mars

At present, supervised classification models are the most common ML applied to Mars. Classification assigns inputs to an output class, and many classification algorithms also include locators that allow the network to both classify the content of an image and locate the extent of the target, either by drawing a bounding box, masking, or segmenting the target [67,74–76]. The development of feature-pyramid networks [66,77–81] has been very powerful as they allow networks to be scale-invariant; the network can recognize an object such as a basketball whether it fills 90% of an image or just 5%. These network features are especially useful for Martian studies since many targets of interest are spatially distant from each other, and manually locating them is very labor-intensive.

By far the most common application of any ML method to Mars has been to segment and count craters on the surface. Crater counting is a well-established method for estimating the age of planetary surfaces [82–87], first applied to the Moon, and in more recent years, to Mars. There are many studies devoted to crater counting on Mars [88–105]. These papers can be divided in two ways: by the minimum crater detection size, or by the methodology used to extract craters. The most common datasets used in these crater counting studies are global in coverage and relatively coarse in resolution. Crater counting requires both a significant number of craters across a range of diameters and a representative sample of the surface, which explains why the existing emphasis has been on global datasets. Furthermore, smaller craters (up to 100 m in diameter) are less indicative of the age of the surface than larger craters, while simultaneously being more difficult to differentiate from secondary craters caused by a larger primary impact [86,106–108]. In some recent work, efforts have even been made to classify craters as "preexisting" or "new," to identify craters that have formed in the last ~15 years [105].

The Mars Odyssey Thermal Emission Imaging System (THEMIS) daytime infrared (DIR) dataset, with a resolution of ~100 m per pixel [109], is the most comprehensive and commonly used imagery dataset [91–93,96,98], while the Mars Global Surveyor Mars Orbiter Laser Altimeter (MOLA) [110], with a resolution of 463 m/pixel, is the most commonly used digital terrain model (DTM) dataset [94,95,111,112]. Recently, data from MOLA and the Mars Express High-Resolution Stereo Camera (HRSC) have been blended to create a global DTM at a ~200 m/pixel resolution [113], which has begun to be used in studies [89]. Other recent work has explored the potential for using even higher-resolution data from the Mars Reconnaissance Orbiter (MRO) High Resolution Imaging Science Experiment (HiRISE) (~0.5 m/pixel) or Context Camera (CTX) sensors (~6 m/pixels) [101], with transfer learning to adapt pretrained crater locators to new datasets. The two most common methods for extracting craters can be simplified into: (1) looking for the characteristic circular crater patterns in imagery and fitting a diameter to each crater, or (2) using elevation data to look for circular depressions and fitting a diameter to each crater. Both methods have proved successful, helping to constrain the ages of large-scale Martian provinces.

The next most frequently used application of ML for Mars is segmenting features in Mars rover imagery. Many studies focus on segmenting or classifying rocks and surfaces nominally, which works toward the goal of optimizing traversability [114–122], while others further group terrain classes as safe or unsafe for rovers [123]. Beyond this, work has focused on segmenting dust storms using MOC imagery and neural networks [124,125]. Some studies have extracted volcanic features using elevation data [126] or HiRISE imagery [127]. Gravity-driven processes are also an area of focus, including recurring slope lineae [128–130] and rockfalls [131,132]. Aeolian features have been the subject of several studies using HiRISE or CTX data, including transverse aeolian ridges (TARs) [127,133] and dunes [134,135] (two of these projects leveraged transfer learning with pretrained versions of RetinaNet [133] and AlexNet [135]). Besides distinct features, efforts have also been made to develop general terrain classifiers for the surface of Mars with broad categories [119,133,136,137]. Looking below the surface, data from the MRO shallow radar (SHARAD) sensor have been used to train a neural network to locate discontinuities in the subsurface [138].

2.1.2. Regression

Unlike the discrete categorization of classification models, regression models connect inputs to continuous outputs. Supervised regressions have been used in studies of Mars, but to a much more limited extent than classification models.

One study [139] used a supervised regression model to predict the true weight percentages of SiO_2, Na_2O, and K_2O as derived from sample data from the laser-induced breakdown spectroscopy (LIBS) ChemCam instrument [140–143]. The samples collected from LIBS did not represent the true overall composition of the sampled rock so the model learned to correct for under- and oversampling caused by the data collection method. The corrected weight percentages were then used in a supervised classifier to predict the total alkali-silica classification of the sampled rocks. Another study used supervised regression models to hindcast the conditions of Mars' thermal evolution using current observations and a large number of simulations [144,145]. This model approach modified parameters representing past conditions, which were then fed into the simulations. The results were compared to current observations, with the model attempting to modify past parameters to better fit the modern observations. By testing an extremely large number of simulations and parameter combinations, the past parameter space that could produce the current conditions could thus be indicated. A final study trained a model to predict five solar wind variables from three spacecraft-measured parameters using data from the Mars Atmosphere and Volatile EvolutioN (MAVEN) spacecraft [146]. In this study, the model was trained on a large amount of past data to learn the relationships between the five dependent and three measured variables.

2.2. Unsupervised Learning

Unsupervised learning uses unlabeled data to generate inferred—rather than explicitly defined—classifications or mappings of the input data, which can help provide insights into the data [147]. Perhaps the most common form of unsupervised learning comprises clustering algorithms such as K-nearest neighbors [148–151], self-organizing maps [152–155], and mixture models [156–163]. Other common applications are in anomaly detection, where a model can identify a data point that is significantly different from the rest [162,164–167].

Unsupervised learning is much less common in Martian research. This is likely due to the tradeoff in unsupervised learning: while it is easier to generate a training dataset (no manual labeling is required) and the algorithms are generally very fast, it is more challenging to align a research goal with the output of an unsupervised algorithm. For example, when an unsupervised algorithm is asked to create a number of classes, it may split or group the data in unexpected or unclear ways. An unsupervised algorithm could naively conclude that a Red Delicious apple is more similar to a tomato than to a green Granny Smith apple. Only with a priori information could the algorithm connect the two types of apple.

Unsupervised learning is used in popular dimensionality-reduction methods such as principal component analysis [168–171] or autoencoders—a type of neural network that can compress input data into a smaller but still representative version of the dataset [172–175]. These unsupervised methods are frequently used in preprocessing pipelines of supervised methods as they can reduce the computation time by reducing the number of parameters in the data and also help mitigate "the curse of dimensionality" [176–180].

2.2.1. Clustering

Most clustering on Mars is carried out using spectral applications [181–183]. In early work [181], unsupervised clustering was used to verify that the spectral responses of data formed two distinct populations, i.e., that the two different sampling areas had different mineral compositions. In subsequent work [182,183], a two-layer Gaussian mixture model was used to decompose spectral responses into the probable component minerals, resulting in the likely detection of rare mineral phases. A recent application [184] of clustering grouped similar rover MastCam [185–187] images.

2.2.2. Anomaly Detection

To date, four published papers [43,136,188,189] and one recent preliminary blog post [190] have focused on anomaly detection on the Martian surface. Some of the published work [43,136] does not use typical "anomaly detection" ontology, and instead, is similar to the general supervised surface classification outlined above. However, one study used anomaly-based detection to identify time-series changes in Martian imagery [188], and another used an anomaly-detection algorithm to discover a water-ice annulus around the north polar region of Mars [189]. The blog post was focused on detecting human-caused disturbances on the surface of Mars such as from rovers or lander impacts. It used a DCNN to locate six examples of anomaly disturbances among 10,000 sample images [43].

2.2.3. Dimensionality Reduction

An interesting application of dimensionality reduction is for testing whether manually extracted features contain meaningful, but disparate, information. A recent paper [191] tested different properties of landslides on Mars such as the slope angle, slide length, and thermal inertia, and similar work has been carried out on Earth-based DTMs, examining the characteristic properties of cirques [192]. Besides this, other Mars researchers have used principal component analysis and sensitivity analyses to identify the most influential features in their data as a preprocessing step, including identifying issues with data transmissions from Mars [193], segmenting Martian dust storms in satellite imagery [124,125], and a rover-based terrain classifier [116]. In the MastCam paper noted above [184], an autoencoder was used to project the rover images into latent space where a k-means classifier could be applied.

2.3. Semi-Supervised Learning

Semi-supervised learning is a hybrid form where both labeled and unlabeled data are used as inputs [194–196]. Typically, there are fewer labeled examples than unlabeled ones.

At its core, semi-supervised learning includes human expertise in labeled data-processing without requiring that time be spent labeling every image or data point. Semi-supervised algorithms are stable and efficient, but sometimes suffer from lower accuracies than other methods [197,198].

Classification

At present, semi-supervised learning is not widely used to study Mars. Two published studies have applied this method [199,200], both using contrastive learning [201,202] and Curiosity rover imagery. Contrastive learning uses a unique optimization function to maximize the agreement between two disparate views of the same target, for example, an image of an entire dog and a cropped image of just a dog's head [201,202]. Wang et al. [199] found that supplementing their labeled training data (Mars Science Laboratory (MSL) Surface Dataset [203]) with 34,000 unlabeled images allowed their image classification model to outperform a baseline model [135] trained on just the labeled data, with nearly 30% greater accuracy across 24 classes. A more recent paper [200] also used contrastive learning to segment MSL imagery. In this study, 16,000 images segmented in six classes were fed into a network that used a semi-supervised contrastive pretraining method. The contrastive pretraining approach boosted accuracy scores by 5–7% overall, but greatly improved the recall score by up to 70% for the smallest minority class that comprised only 0.03% of the dataset's pixels. Large improvements on rare classes are difficult to achieve, so these results are very promising.

2.4. Self-Supervised Learning

Self-supervised learning is intermediate between supervised and unsupervised learning. In self-supervised learning, unlabeled data are the model input while the outputs are typically classified in some way. For example, natural learning processing (NLP) models may be fed huge amounts of text with random portions masked out to train a network to derive the content and structure of a language from context [204–207]. Perhaps the most well-known application of self-supervised learning in image processing is in generative adversarial networks (GANs) [208–210], which have become increasingly powerful in recent years with the development of user-friendly off-the-shelf networks such as StyleGAN [211,212]. These systems use two networks to generate synthetic data within the latent space of the training data: one network learns to generate synthetic data, while the other network learns to discriminate between real and synthetic data. This adversarial learning process improves both networks simultaneously. Common applications of GANs include the generation of photo-real artificial human faces [211–215], images based on input text descriptions [216–220], and "super-resolution" or upscaled images in many domains [221–228].

The training of these upscaling models is relatively simple: a downsampled image is used as the input and a higher-resolution image is used as the target. These image pairs are used to train the model to infer the upscaling needed to generate the target resolution. The trained network can then be given a base-resolution image, and the model will generate "missing" data to increase the input image's resolution. This method can also be used to add color to panchromatic imagery or to fuse data from different sources [229,230].

Two separate projects have focused on generating super-resolution imagery of Mars, one focused on satellite imagery [231] and another on rover imagery [232]. In the satellite project, the network was trained on pairs of downsampled and corresponding full-resolution HiRISE images; in essence, the network learned to recreate higher-resolution HiRISE images from the lower-resolution alternatives. The model was then applied to the Color and Stereo Surface Imaging System (CaSSIS) instrument data (via transfer learning) to generate higher-resolution multi-spectral optical imagery with an approximately three times greater resolution. The rover work was similar in that pairs of degraded and original images were fed in, and the model then learned to generate higher-resolution surface images, which in theory, could be useful for further studies.

Another GAN, dubbed MADNet, has been developed to generate high-resolution digital terrain models (DTMs) from imagery [233–235]. The most recent version, MADNet 2.0 [233], can generate accurate DTMs from just HiRISE imagery with a 16 to 100 times greater resolution than dedicated DTM instruments can produce. The network was compiled with pairs of downsampled HiRISE images (input) and their corresponding DTMs derived from stereo HiRISE coverage (target). The model was then trained to recreate the full-resolution DTMs from the lower-resolution images. The final model could generate a native-resolution DTM for any HiRISE image.

One self-supervised project that did not use GANs was for a rover-based self-supervising terrain classifier that combined imagery and wheel vibration data to classify terrain as safe or unsafe based on the rover's experience in the environment [236]. However, due to technical limitations, the success of the project was limited (precision scores of ~70%, 10–15% worse than a supervised classifier), and it is difficult to compare these early attempts to modern ML methods with more complex architectures and vastly greater computational power.

3. The State and Future of Machine Learning on Mars

3.1. Why Use Machine Learning at All?

When evaluating the possibilities for ML applications on Mars, it is important to first note a number of important differences between terrestrial geomorphic applications of ML and those found on Mars. These differences may in part explain why ML, using current approaches, may be difficult to apply to the range of Martian surface-feature identification issues, as well as to applications associated with spacecraft landing and traversing the Martian surface. Owing to the issues that will be presented in this section, geomorphic predictions from ML may have "low resolution", and thus may offer weaker results than from ground-based sampling or mapping [237]. That said, many exciting potential applications may produce new insights into Martian geomorphic and climatic evolution, generating valuable information for future exploration work.

First—and probably most important—among the constraints on ML applications is how researchers are dealing with a surface and subsurface that cannot be exhaustively sampled in situ. There is, unlike terrestrial features, no true "ground truth" for Martian landforms. We begin with assumptions about what the features are without physically examining those features to determine the source processes. Therefore, many interpretations start with a level of uncertainty that is quite different from when studying terrestrial environments where scientists can physically examine the surface themselves. On Earth, human-derived samples or observations are often complex and ambiguous, and there can be problems with spatial and temporal extrapolation [238]. These issues are exacerbated on Mars, where the classification of features on the Martian surface tends to be poorly constrained relative to terrestrial research. Plus, in many, if not most, instances on Mars, geomorphic processes cannot be directly observed, and remnant features may reflect processes no longer active [239].

Second, physical processes on the Martian surface, like those on other planetary bodies, are controlled by basic physics and chemistry. Therefore, ultimately, the manifestation of Martian surface features should be predictable if the underlying physics and chemistry are well-known, meaning training datasets that reflect these physical properties can be developed. Balaji when discussing the use of ML in the physical sciences, noted that in recent research, it is assumed that everything can be derived from the first principles of classical physics [240]. Along these lines, Church noted that the intention of modern geomorphologists in seeking to understand landscapes is to "interpret features in terms of observables by the application of Newtonian mechanics." [241]. However, currently on Mars, this is not directly possible, except at a few sites where rovers could sample in situ. Remotely sensed physical and chemical details of the Martian surface, while available and of value, are somewhat indeterminate and fuzzy. Learning algorithms, while capable of producing interesting results from these training datasets, must respect physical constraints, even if they are not present in the data. This may be one reason why unsupervised learning, relative to other types of ML, has been scarcely applied to Martian features. Unsupervised learning uses unlabeled data to generate inferred—rather than explicitly defined—classifications or mapping of the input data, which can help provide insights into the data. Unsupervised learning is, therefore, both a blessing, in that it may identify groupings of objects that might not occur to an observer with terrestrial analogs as a guide, and a curse, in that these groups may be meaningless or uninterpretable.

Third, even at sites where rovers could sample, there may be significant differences in the interpretations of geomorphic and geologic processes and resultant landforms. For example, studies of the source processes of deposits sampled by the Curiosity rover in the Gale crater produced conflicting hypotheses—lacustrine versus aeolian—about the formation of these sedimentary deposits [242–245]. In many cases, different processes can produce similarly appearing deposits that may be difficult, if not impossible, to differentiate. This equifinality, where the same end state may be achieved via many different paths or trajectories [238,246], produces great uncertainty. For example, rock glaciers on the north side of Mount Sharp in the Gale crater [247], while having a similar appearance to rock glaciers on Earth, could also be produced by subtle differences in driving processes (mudflow, lahar), leading to similarly appearing forms. As geomorphic researchers have noted [237,239,248], interpretation in geomorphology is inherently indeterminate, with "combinations of attributes, relationships, processes, drivers, legacy effects and sequences of events creating contingent circumstances that fashion complex arrays of responses" [237]. As such, considerable error can result from applying generalizations to specific cases, and a lack of objectivity may severely affect training dataset creation and subsequent interpretation [237].

Fourth, many Martian features have no known analog on Earth. Transverse aeolian ridges (TARs) are an excellent example where a feature that appears much like a transverse dune at a large scale, and a ripple at a small scale, is actually neither and without a clear analog on Earth [249–260]. This makes conceptualization of ML approaches difficult and interpretation of results unclear. As [240] noted, "one can have understanding of the system without the ability to predict; one can have skillful predictions innocent of any understanding. One can have a library of training data, and learn the trajectory of the system from that, at least in some approximate or probabilistic sense. If no analogue exists in the training data, no prediction is possible." Held noted that to pass from simulation to understanding, ML-based modeling must learn from data comprising not just patterns but also simpler models [261]. In many cases, the requirement for models and associated training sets may necessitate the production of training sets with attributes that are more appropriate than simple bounding-boxed examples.

Finally, most landforms are typically not discrete objects and lack universally applicable definitions, with such a definition relying on an "I know it when I see it" type of expertise. Geomorphic features typically have fuzzy ill-defined boundaries that grade into other features (e.g., hill-to-valley). For example, cirques normally found in mountainous environments are generally defined as a semicircular feature with a steep head and sidewalls, an over-deepened central area, and a low sill that defines the lower edge of the feature. However, the poorly defined lower edge often grades into a talus slope, and the upper edges may take the form of a sharp arête or a poorly defined break in the slope [192]. Even when the prescribed features are present, the "edges" of the feature may be diffuse/transitional. Measures of cirque size and form can thus vary from observer to observer [192,262]. Nonetheless, even with these uncertainties, a relative novice mountaingoer can recognize a cirque. As such, while robust and verified algorithms can objectively and repeatably identify crisply defined objects, these identifications are currently lacking in the geomorphic realm.

3.2. Future Machine Learning Studies on Mars

It is important to note that until recently, only relatively low-resolution data were available for analysis of the Martian surface. This resulted in the creation of poorly constrained training datasets ill-suited to analyzing all but the largest surface features. Now though, ML approaches can be used to optimize data extraction from relatively new high-resolution sources, to explore properties of the surface and its change over time that were until relatively recently of sub-pixel resolution. As [16] suggested, "To acquire observational data related to mapping and timing of activity, continued high-resolution orbital imagery is key." The following sections of this article highlight specific areas of research that could benefit from applying existing methods to the higher-resolution imagery.

3.2.1. Mission Planning and Landing

Mission planning considerations relate to fuel management, communications stability, guidance quality, the selection of geologically interesting landing sites, and landing site safety. ML has been increasingly applied to these issues, specifically in detecting telemetry issues [193,263–265], managing fuel/power [266,267], developing guidance systems [268–271], determining safe landing conditions (discussed in detail below), and selecting landing sites (discussed elsewhere in this review), among others [272].

Landing a spacecraft on a plain cluttered with boulders presents multiple problems, including threats to the lander safety and rover trafficability for subsequent scientific exploration [273–282]. This topic has been especially well-studied for Mars, where boulder fields have been a serious concern for landers. While multiple successful landings on Mars have taken place, an entire mission can be terminated due to rocks at the landing site. The challenge in overcoming this issue includes characterizing the boulder distribution (ideally, to identify areas with smaller boulder densities) and surface roughness during pre-mission site selection [275,279,283–287], and then, again during the entry, descent, and landing stages of a mission [280,286]. Enhanced recognition of boulders and other surface roughness obstacles is critical for mission success and subsequent exploration. Boulder fields are best resolved in HiRISE imagery, and the previous works cited in this section all used HiRISE data. In the future, more advanced supervised classifiers could be developed to help solve the problem of recognition, and data fusion between greater sensor types, such as those producing thermal inertia and elevation data, could be used as an additional feature to derive lander safety maps.

3.2.2. Boulder Sampling Strategies

Understanding the distribution of boulders and their properties is of significant importance since the boulder size-frequency distribution is critical for understanding the surficial geology, sedimentology, and erosional/depositional processes on Mars. The Perseverance rover landed in the Jezero crater in 2020 and will soon be sampling the deltaic deposits within the crater for sample return and evaluation of potential past life on Mars. A sampling strategy [288,289] was designed to collect samples that are both readily accessible in situ, as well as materials that may originate from boulder falls from the inaccessible upper surface of the delta, which contains a collection of boulder debris from the delta drainage catchment. [290] developed a customizable algorithm for boulder extraction under different brightness and contrast levels and illumination angles that can be used for sample selection, and various other methods for extracting boulders also exist [279,280,286]. Similar preplanning studies are necessary for future missions to Mars with other objectives and criteria [291–293]. In these studies, anomaly detection and supervised classification algorithms could be used to identify, locate, and then map boulders on the Martian surface using HiRISE data, to produce maps that could then be used in geological and geographic analyses.

3.2.3. Identify Shorelines and Deltas

Extracting high-water marks and deltas related to an ancient global ocean [294–296] and paleolake shorelines [297,298] is critical to understanding Mars' climatic history. While the largest of these features are easily discernable in satellite imagery, most are typically subtle features on the landscape, subject to interpretation issues. A supervised classification algorithm could be trained to locate deltas and/or terraces in HiRISE imagery, but terraces would likely be easier to identify in high-resolution DTMs.

3.2.4. Map Unusual Aeolian Features

Transverse aeolian ridges (TARs) are wind-created landforms unique to Mars [254,255,257–259,299–302] that may provide insights into the past Martian climate [303], or more importantly, the nature of aeolian features in general across planetary bodies [250,252,304–306]. TARs are sparse but common, whereby TAR fields are small in scale, but frequently occur across the surface of Mars. Manually locating all of these features globally is nearly impossible, although some representative efforts have been made [256,301]. A preliminary study using a supervised classification algorithm identified TARs with high precision [133] in HiRISE imagery, but a global survey is yet to be completed. Information as basic as the density of TAR fields across Mars could provide greatly important insights into the role of the atmospheric density in shaping aeolian features [306,307], as well as the evolution of complex aeolian fields [304]. Other features of interest that could be mapped in high-resolution imagery include periodic bedrock ridges (PBRs) [308–311] and dark dune areas, which may have liquid water and astrobiological significance [312–314]. Supervised classification algorithms or anomaly detectors could be trained to map dark dune areas. Supervised classifiers can identify TARs in HiRISE imagery [133] and could likely be adapted to locate PBRs, as well. Both TARs and PBRs could easily be detected if high-resolution DTMs were more broadly available.

3.2.5. Map Inverted Channels

Inverted channels are raised features interpreted as exhumed fluvial paleochannel deposits exposed by erosion. The inverted terrain represents possible cemented deposits resistant to erosion [315]. Martian channel inversion is the result of long-term aeolian erosion [316,317]. The degree of exposure can be used to determine erosion rates [318–320]. Mapping these features is difficult since most are relatively small and at times indistinguishable from non-inverted surficial channels. These features would be best extracted by a supervised classifier in high-resolution DTMs, but such extraction may be possible with HiRISE data. Once extracted, further analyses of the width, length, or branching patterns of the channels could be performed to better understand historic flow patterns.

3.2.6. Map Small Channels

The amount of water, or discharge, that flowed through Martian rivers can be used to understand the planet's former climate. While large channels have been mapped [321–323], smaller channels, which likely played an important role in past Martian hydrology, are poorly mapped [324]. Small channels are also important when identifying chloride deposits on Mars, which are important since they record the last surface water present at a given location on the surface, seeing as subsequent water events would dissolve them. Chloride deposits are found in local topographic depressions, sometimes with channel-like features that are often at the resolution limits of available imagery. Highly effective and simple tools to extract channels from DTM data have existed for decades, but the lack of high-resolution DTMs is again limiting. Given the likely characteristic pattern of illumination and shadow across channels, they could also potentially be mapped in imagery by a supervised classification algorithm. Then, similar to inverted channels, characteristics of past flow conditions can be inferred from these channels.

3.2.7. Locate and Characterize Chaotic Terrain

Chaos terrain refers to regions of a planetary landscape characterized by irregularly shaped, flat-topped, angular-sided blocks separated by steep valleys [325]. Several hypotheses exist to explain their formation, including association with flooding and outflow channels, crustal deformation, subsurface collapse, and groundwater release [326]. Mapping the distribution of these features through the recognition and classification of Martian chaos terrain could help distinguish theformation mechanisms [327] on Mars, as well as on similar planetary and planetary satellite surfaces [328,329]. The irregular nature of chaos terrain could prove challenging for a supervised classifier, but given the relatively large scale of chaos terrain on Mars, ML applications would not just be limited to HiRISE data; beyond these, classifiers could incorporate greater dimensionality into the dataset by using other instruments with a greater spectral resolution. Given recent advances in ML super-resolution methods [330–333] and standard panchromatic sharpening [334–336], these coarse datasets could be leveraged to help identify patterns of blocks and valleys.

3.2.8. Locate Ice/Water

Thermal and geomorphic mapping would be useful to locate accessible ice deposits within regions located near preferred landing-sites [337]. This ice is typically covered by a layer of dust or regolith, but is exposed in some locations by fresh impact craters or in erosional scarps [338,339]. Like small channels and inverted channels, exposed scarps are small features [338], often at the limits of imagery resolution. As such, supervised classification approaches may be useful to locate and analyze these features, especially since ice and water prompt different responses from Martian regolith, which may be recorded via a range of remote-sensing methods such as thermal, radar, and seismic sensing. Similar approaches, using a range of geophysical sensors, have suggested significant subsurface water exists across much of Mars outside of the polar regions [340].

3.2.9. Identify Glacial Landforms

To return to a previous example, a cirque, normally found in mountainous environments, is generally defined as a semicircular feature with a steep head and sidewalls, an overdeepened central area, and a low sill that defines the lower edge of the feature. However, many features recognized as cirques have one or more of these elements poorly defined or missing. Moreover, even when these features are present, the "edges" of the feature may be diffuse/transitional. Measures of cirque size and form can thus vary from observer to observer. As described above, however, even a relative novice mountain-goer can recognize a cirque. The presence of cirques on Mars indicates both past glaciation and areas of potential for locating subsurface remnant water or ice [341]. Other morphologically distinct glacial features on Mars include U-shaped valleys [192], lineated valley fills [342–345], concentric crater infills [342,343,346,347], and glaciers themselves [247,348]. There has already been success in extracting cirques from relatively coarse DTM data [192,262] with supervised classifiers and simple methods, as well as mapping debris-covered (rock) glaciers with a combination of coarse imagery and DTMs [349–351]. Similar methods should be tested on Mars.

3.2.10. Detect Novel or Rare Mineral Phases

Spectral data from Mars have been used to detect rare mineral phases in the Jezero crater [182,183]. Other rare mineral phases likely exist on Mars, and broader applications of ML methods to mine CRISM data should yield fruitful insights in novel geographic areas of interest for mineral researchers. In general, the application of multi-spectral methods to Mars remains underexploited given the efficacy these methods have demonstrated on Earth [24,352–357]. However, the recent development of an ML toolkit for analyzing CRISM data is a promising step in this direction [358].

3.3. Leverage Generative Adversarial Networks

3.3.1. Generating Synthetic Imagery

Machine learning is challenged by class-imbalance problems [359–365] and limited datasets. Some ML methods will not perform well if a single class is overrepresented within their training data. For example, a network that determines dogs versus cats in images will not work well if it is trained on a dataset composed of 80% cats and 20% dogs as the network can simply guess "cat" for every image and will be correct 80% of the time.

There are well-established methods to mitigate this imbalance in quantitative data, such as the synthetic minority over-sampling technique (SMOTE) [366], but the options are much more limited when it comes to training with complex inputs like images. Recent developments such as focal loss [66] and semi-supervised contrastive training [200] can drastically reduce the effects of class imbalance, but the challenge remains, especially in small datasets where a minority class is very rare, perhaps with only a few dozen examples in a dataset of hundreds. Most ML methods rely on having a wealth of training data to create robust and generalized models, but sometimes a large number of samples is simply not available or is too time-intensive to collect.

Several studies have suggested that GANs could be used to help mitigate both these problems, by either generating synthetic data to supplement minority classes and reduce the imbalance, or by generating more training data from a small dataset [367–369]. Perhaps most relevant to Martian research are recent studies that demonstrate the efficacy of generating synthetic high-resolution remotely sensed data [370–373]. While it may seem counterintuitive to generate more Martian data when so much of the existing data remains unexplored, the ability to generate more data of a specific type or with specific characteristics is a promising tool for future research on Mars.

Synthetic data could help in two ways. First, the use of synthetic data could help mitigate spillage between training, testing, and validation datasets. For example, a terrain-classifying CNN trained on NavCam imagery may have images of the same area of Mars within its training and testing datasets. While the images themselves are unique and taken from different perspectives, there is overlap within the content of the images—perhaps a unique pattern or object can be seen in multiple images. This overlap could artificially increase the performance of the CNN during testing. To overcome this issue, a GAN could be trained to generate synthetic imagery with the same image characteristics as the NavCam imagery (resolution, field of view, optical distortion, etc.) from training data collected elsewhere on Mars by other rovers. Using this additional imagery in the training and/or testing datasets could reduce spillage and help create a more general classifier. To this end, a recent study showed that GANs can create realistic synthetic rover images [374]. This same method could also be applied to satellite-based terrain classifiers. Even if the training and testing datasets are derived from disparate images, there is a possibility that the images have been collected from the same area and may have similar or overlapping content. This risk is especially high with HiRISE data as the narrow coverage and targeted use of the camera means that some areas have extremely dense and/or repeat coverage. In that context, using GANs to generate synthetic terrain could be helpful in both training to make a classifier more general, and in testing to ensure independence between the datasets.

Second, class-imbalance problems and limited datasets are an issue on Mars, particularly the latter. HiRISE data only cover 3% of Mars, so features that are rare on Mars are likely to be extremely rare in high-resolution imagery. The small number of features could prohibit automated classification and location, though they support anomaly detection. GANs could be used to generate additional examples of the features to train a supervised classifier. For example, recurring slope lineae (RSL) were first described in 2011 in seven locations [375], and in the years since, 933 more locations have been manually identified [376]. There is little reason to believe that every imaged occurrence of an RSL has been identified, and GANs could help increase the training dataset for a CNN-based locator-classifier, which could then find further RSLs. In a promising study [377], Wang et al. showed that a classifier trained with ~900 examples of RSLs was highly (92%) accurate in locating RSLs in 136 other instances; looking ahead, this method could be improved and generalized with additional data augmentation. When testing the feasibility of the approach, the authors of this review found that StyleGAN could be trained to create realistic HiRISE data with just consumer hardware in a preliminary implementation (Figure 1) [378].

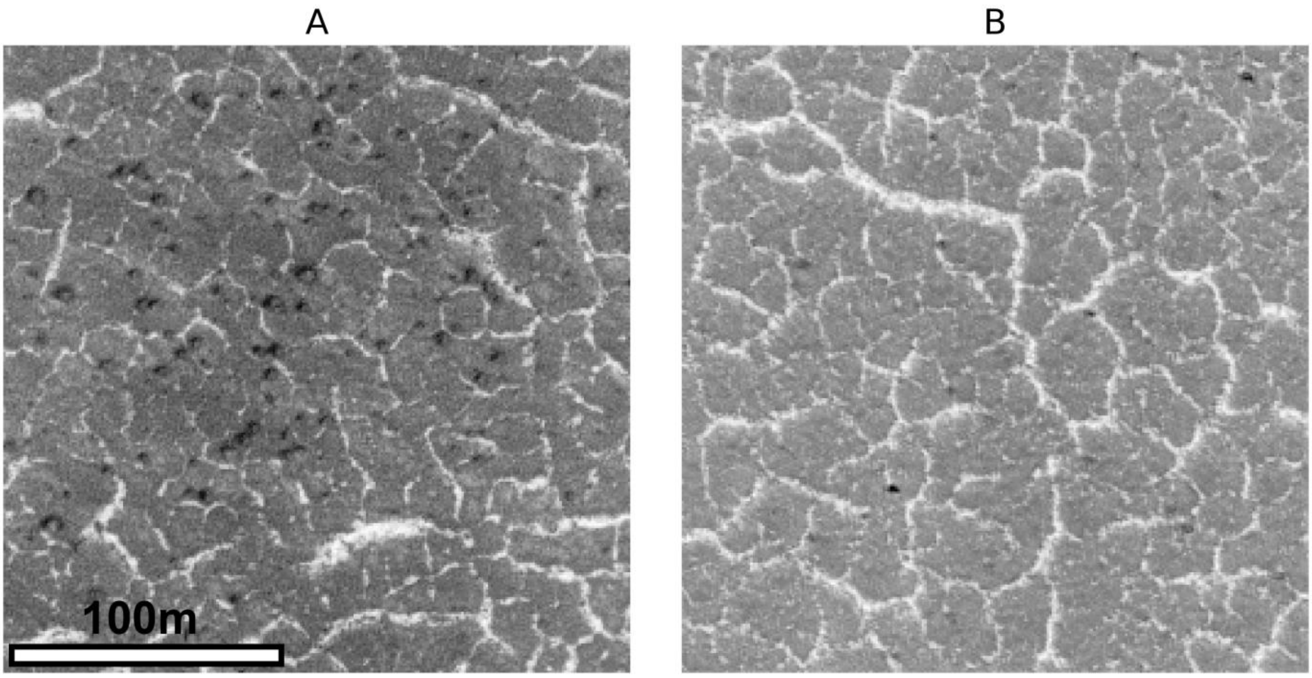

Figure 1. Synthetic imagery of polygonal terrain on Mars. (**A**) Real HiRISE imagery, (**B**) synthetic image generated by a trained StyleGAN network. Resolution for both images is 0.5 m/pixel.

3.3.2. Feature Extraction from DTMs

DTMs of Mars are limited in either resolution or coverage, but are vital tools for planetary scientists. There are a wealth of Earth-based studies and methods for extracting geomorphological information from DTMs, but the domain transfer of these methods to Mars has been limited by the small number of high-resolution DTMs available. While early work in this field was promising [379,380], recent efforts have stalled.

The HiRISE instrument can create 0.5–1 m-per-pixel DTMs from stereo imagery, but at present, only ~0.3% of Mars has stereo coverage, and less than one-tenth of those scenes have DTMs generated. The recent development of high- and super-resolution synthesized Martian DTMs [233–235,381] has the potential to revolutionize Martian geomorphology in years to come.

A wide range of geomorphological features and landforms have already been shown to be identifiable and extractable from DTMs. The general methods were covered in various reviews [382–393], but those applicable to features specifically relevant to Mars (see Section 3.2) are as follows: rock glaciers [350], glacial terraces and ridges [394], glacial cirques [192,262], polygonal terrain [395–397], drumlins [386,398,399], glaciovolcanic features [400,401], landslides [402–405], deltaic features [406], watersheds [407], loess features [382,408], karst landscapes [409,410], relict patterned ground [411], fluvial terraces [412], and thalwegs [413].

Besides those established in terrestrial studies, a further range of potential applications is specific to the Martian domain. Boulders, for instance, could be automatically extracted from DTMs to help determine the rover-landing safety, classify ancient shorelines, or delineate geologic units [273,274,276,277,279,284,414–416]. More accurate profiles and measurements could be made of small-scale features such as TARs [299–301,417] PBRs [308], and models could be trained to map their locations and sizes automatically [133,259,417]. Inverted channels are important markers of past fluvial activity, and their distinct topographic characteristics [316,317,418–420] could be automatically detected. The mapping of channels too fine to be resolved at current DTM resolutions could be made possible in this same way.

Further theoretical applications could include the verification of human-imposed classification schemes by unsupervised classifiers. For example, an unsupervised classifier could group high-resolution data from craters to assess expert-estimated weathering and erosion patterns (i.e., young, old, and very old craters). If the classifier consistently grouped craters with low estimated ages separately from those with high estimated ages, this would support the use of those markers for age estimation. Similar verification experiments could be performed on other top-down classification schemes.

3.4. Develop Standardized Datasets

Standardized benchmark datasets are crucial to quantify the current state-of-the-art methods across studies. There are innumerable benchmark datasets in nearly every field in the literature, and many have been used in hundreds or even thousands of studies [421–446]. For example, the MNIST database of handwritten digits [443] has been cited in over 5700 publications at the time of writing. Besides serving as useful prototyping tools, these datasets serve a very important purpose in allowing one-to-one comparisons of different methods. At present, only a handful of standard datasets exist for Mars, and new methods are rarely directly compared to existing methods. Looking ahead, we propose that a standard testing dataset containing both imagery and DTMs should be created for crater counting methods. Then, as new algorithms or approaches are developed, their performance and characteristics can be directly compared. Currently, there is no easy way to determine which crater counting method performs the best out of the dozens outlined here. Without this comparison, every researcher has reason to believe that their method is the best, and a method may become the standard in related studies out of habit rather than by merit. As the use of ML expands in planetary science, the need for these resources will increase, and funding for their creation should be a priority.

3.4.1. Unlabeled Data

The most popular standardized dataset is Mars32k [447], which has been used in several studies, primarily those focused on rover navigation [123,232,374]. The dataset is relatively simple and is intended for unsupervised learning projects. As the name implies, it contains 32,000 images that have been downsampled via linear interpolation to a standard resolution of 560 $\times$ 500 pixels. The uniformity of the data and the dataset's ease of use are commonly cited reasons for its popularity. As discussed above, unsupervised learning is not commonly utilized in Martian studies, but more unsupervised research is warranted; to advance unsupervised research in this way, the community needs more unlabeled datasets.

3.4.2. Expert Labeling

Most of the existing benchmark datasets on Mars are derived from expert knowledge, but few have achieved widespread use. The GSMRI dataset [374] used Mars32k and a GAN to generate synthetic images of Martian rocks, thereby doubling the size of the dataset, with a four-level classification structure used to label all rock images. Meanwhile, the DoMars16k [137] dataset consists of 16,150 samples across 15 general landforms in five categories, derived from 163 Context Camera images [448]. Further to this, AI4Mars [449] contains 35,000 images with 326,000 labeled objects intended for use in training autonomous rover navigation algorithms. Elsewhere, Rockfall Mars and Moon (RMaM) [450] contains a mixture of Martian and Lunar satellite images that can be used to train and test rockfall detectors. Then, the Mars orbital image (HiRISE) labeled data, version 3.2 [451], contains 10,815 samples broken down into eight landform classes. In another example, the MSL Surface Data Set (v2) contains 6800 images with 24 classes that are mostly focused on parts of the Curiosity rover as well as rover activities. The Mars day crater detection (MDCD) dataset, meanwhile, is composed of 500 images and 12,000 craters [88].

The datasets of rover imagery are at present very good; however, creating more satellite image-based datasets should be a priority. Satellite images cover a more diverse geographic distribution than rover images, and they are useful in wider domains. However, labeling satellite imagery is challenging given that a single satellite image can cover a large spatial extent and include many different types of features that might need to be re-labeled or reclassified for different projects. For example, a broad "aeolian" class might be suitable for one classifier model, but another might need subcategories [249] such as "dunes" and "ripples," while a third project might need to identify different types of dunes. Thus, experts' efforts to develop a more unified supervised classification hierarchy represent an important endeavor; to date, certain work has been done in this area of semantics by looking at DTMs on Earth [452]. Recent work also identified this problem and used semi-supervised learning as a solution [199,200,452], but a consensus structure should remain the priority.

3.4.3. Crowd-Sourced Data Labels

There have been a few projects seeking to leverage "the wisdom of the crowd" to classify Martian images: LabelMars [453,454] (as part of the Novelty or Anomaly Hunter (NOAH) project [455]), AI4Mars [449], Content-based Object Summarization to Monitor Infrequent Change (COSMIC) [456,457], Planet Four [458–460], and Planet Four: Ridges [461,462]. LabelMars was unable to recruit enough volunteers to succeed, and it reverted to an expert-labeling method. AI4Mars used the same dataset and successfully collected a significantly larger number of labels, likely due to the much simpler classification scheme of six classes, versus 20 in LabelMars. COSMIC generated 151,000 classifications from 4240 volunteers using a simple scheme to mark and classify araneiforms [463] in HiRISE imagery near the south polar region [456]. Planet Four generated 279,000 classifications from 16,734 volunteers searching for carbon dioxide jets in HiRISE imagery [458]. Planet Four: Ridges generated 514,000 classifications from 14,079 volunteers using a simple two-class system to locate polygonal and Meridiani-type ridges [461].

Given the huge quantity of data from Mars, using novice or amateur classifiers is an important direction for future work. Non-experts can help expand existing datasets or may contribute to generating novel ones. These datasets can then be used for research directly or work as training datasets for ML classifiers. The classification schemes used in the expert labeling section above were all relatively simple and accessible to non-geologists. The infrastructure for crowd-sourcing image labels and classifications is available on many web-based platforms such as Zooniverse [456,458,461] and LabelBox, and the growing public participation appears to demonstrate an appetite to help, making this an area ripe for further development.

3.5. Unify Geographic Data and Analysis Systems

The Planetary Data System (PDS) [1,2] is a distributed data storage and access system used to house NASA data from rovers, satellites, and other instruments. Data in seven categories (atmospheres, small bodies, etc.) are stored at different "nodes" across the United States, usually hosted by a university or other major institution. These nodes use different website structures, data formats, search queries, and tools—demanding practice and experience with each system. Further complicating the data navigation is the stratification of different products across different nodes. For example, the final one-meter DTM for the Gale crater can be found on the "cartography" node hosted by the United States Geological Survey, while the data the DTM is derived from are found there but also on the "geosciences" node hosted by Washington University in Saint Louis. Interactive maps showing the spatial distributions of these data are then hosted separately on the websites of Arizona State University (MOLA, HRSC), and the University of Arizona (CTX, HiRISE). If one wanted to use this DTM with the ground or atmospheric temperature in the Gale crater, the data could be found on the "atmospheres" node hosted by New Mexico State University, but there is no equivalent map visualization to locate ground or atmospheric samples that spatially overlap with the DTM in question. While there are certainly benefits of this distributed system, the disparities between different instruments' workflows and data storage make cross-disciplinary research challenging to all but the most experienced users. As noted by [16], such research is key to advancing our understanding of planetary surface processes: "We need coupled surface, subsurface, and atmospheric/meteorological measurements so as to enable 'full system' studies."

As large corporations grow increasingly interested in planetary-scale data products (e.g., Google Earth and Microsoft's Planetary Computer, among many smaller competitors), the disparity between these holistic solutions and the PDS grows. Google Mars is a popular platform that enables many Martian datasets and basemaps to be visualized at once. By using an extension of the Google Maps application programming interface (API), users can query several basemap types: elevation, visible, and infrared. However, the API is outdated compared to that of Google Earth Engine, and it lacks the high-resolution products that have revolutionized Martian science in recent years. JMARS [464] is another excellent geographic information system designed specifically for Martian data by Arizona State University. While JMARS works with most of the common geoscience data products, it does not yet include other data such as atmospheric information or raw imagery. Furthermore, it lacks a robust API for large-scale programmatic analyses. At present, neither platform could answer a query such as "return a list of all HiRISE DTMs that overlap >50% with CTX DEMs." Funding to refine these existing tools, or develop new, more comprehensive platforms, should be a priority to enable further ML studies of Mars.

4. Conclusions

The collection of Martian data has outpaced the rate at which humans can meaningfully parse and interpret each record. Leveraging the novel automated analysis methods pioneered in other fields—Earth observation, most notably—presents a natural solution to this dilemma. As we have outlined in this article, ML studies are taking place on Mars, and there are many fruitful avenues via which these could be further applied. As [16] recently noted, "Mars is a uniquely enabling study target for investigations of surface processes active on other planetary bodies—both for extending terrestrial based process models and, in some areas, for serving as a superior comparative planetology basis over Earth."

With greater knowledge transfer between Martian domain experts and machine learning specialists, insights from ML research could increase. Here, we outlined a range of specific future study routes, and we offered a few broad suggestions for the community and research funders. We conclude that improvements to our understanding of the physical processes on Mars, and potentially other non-terrestrial surfaces, can be achieved using ML. A few key findings should be noted: (1) semi-supervised and self-supervised learning are especially important methods for Martian applications, (2) creating synthetic Martian data (especially of high-resolution, accurate digital terrain models) using generative adversarial networks has the potential to revolutionize Martian geomorphology studies, (3) developing standardized datasets and benchmarks with which to test new methods should be both a research and funding priority, and (4) Martian research is hindered today by the lack of a scalable and programmatic analysis platform, such as Google Earth or Planetary Computer.

Challenges aside, existing and ongoing ML research on Mars has proven valuable, and the research and methods summarized here should be used as a basis to fund, encourage, and undertake further such studies.

Author Contributions: Conceptualization, T.P.N.-M., L.A.S. and N.E.; writing—original draft, T.P.N.-M.; writing—review and editing, T.P.N.-M., L.A.S. and N.E. All authors have read and agreed to the published version of the manuscript.

Funding: This research received no external funding.

Institutional Review Board Statement: Not Applicable.

Informed Consent Statement: Not Applicable.

Data Availability Statement: No novel data were produced for this review.

Conflicts of Interest: The authors declare no conflict of interest.

References

1. Hughes, J.S.; Li, Y.P. The Planetary Data System Data Model. In Proceedings of the Twelfth IEEE Symposium on Mass Storage Systems, Monterey, CA, USA, 26–29 April 1993; Institute of Electrical and Electronics Engineers (IEEE): Piscataway, NJ, USA, 1993; pp. 183–189.
2. McMahon, S.K. Overview of the Planetary Data System. *Planet. Space Sci.* **1996**, *44*, 3–12. [CrossRef]
3. Arviset, C.; Dowson, J.; Ortiz, I.; Parrilla, E.; Salgado, J.; Zender, J. ESA Planetary Science Archive. In *Astronomical Data Analysis Software and Systems XVI.*; Astronomical Society of the Pacific: San Francisco, CA, USA, 2007; Volume 376, p. 163.
4. Macfarlane, A.J.; Docasal, R.; Rios, C.; Barbarisi, I.; Saiz, J.; Vallejo, F.; Besse, S.; Arviset, C.; Barthelemy, M.; de Marchi, G.; et al. Improving Accessibility and Discovery of ESA Planetary Data through the New Planetary Science Archive. *Planet. Space Sci.* **2018**, *150*, 104–110. [CrossRef]
5. Estlin, T.A.; Bornstein, B.J.; Gaines, D.M.; Anderson, R.C.; Thompson, D.R.; Burl, M.; Castano, R.; Judd, M. Aegis Automated Science Targeting for the Mer Opportunity Rover. *ACM Trans. Intell. Syst. Technol.* **2012**, *3*, 1–19. [CrossRef]
6. Francis, R.; Estlin, T.; Doran, G.; Johnstone, S.; Gaines, D.; Verma, V.; Burl, M.; Frydenvang, J.; Montaño, S.; Wiens, R.C. AEGIS Autonomous Targeting for ChemCam on Mars Science Laboratory: Deployment and Results of Initial Science Team Use. *Sci. Robot.* **2017**, *2*, eaan4582. [CrossRef] [PubMed]
7. Estlin, T.; Castano, R.; Bornstein, B.; Gaines, D.; Anderson, R.C.; de Granville, C.; Thompson, D.; Burl, M.; Judd, M.; Chien, S. Automated Targeting for the MER Rovers. In Proceedings of the 2009 Third IEEE International Conference on Space Mission Challenges for Information Technology, Pasadena, CA, USA, 19–23 July 2009; Institute of Electrical and Electronics Engineers (IEEE): Piscataway, NJ, USA, 2009; pp. 257–263.
8. Johnson, A.E.; Cheng, Y.; Montgomery, J.F.; Trawny, N.; Tweddle, B.; Zheng, J.X. Real-Time Terrain Relative Navigation Test Results from a Relevant Environment for Mars Landing. In Proceedings of the AIAA Guidance, Navigation, and Control Conference, Kissimmee, FL, USA, 5–9 January 2015; p. 851.
9. Wolf, A.A.; Acikmese, B.; Cheng, Y.; Casoliva, J.; Carson, J.M.; Ivanov, M.C. Toward Improved Landing Precision on Mars. In Proceedings of the 2011 Aerospace Conference, Big Sky, MT, USA, 5–12 March 2011; Institute of Electrical and Electronics Engineers (IEEE): Piscataway, NJ, USA, 2011; pp. 1–8.
10. Owens, C.; Macdonald, K.; Hardy, J.; Lindsay, R.; Redfield, M.; Bloom, M.; Bailey, E.; Cheng, Y.; Clouse, D.; Villalpando, C.Y. Development of a Signature-Based Terrain Relative Navigation System for Precision Landing. In Proceedings of the AIAA Scitech 2021 Forum, Virtual, 11–22 January 2021; p. 376.
11. Johnson, A.; Aaron, S.; Chang, J.; Cheng, Y.; Montgomery, J.; Mohan, S.; Schroeder, S.; Tweddle, B.; Trawny, N.; Zheng, J. The Lander Vision System for Mars 2020 Entry Descent and Landing. In Proceedings of the AAS Guidance Navigation and Control Conference, Breckenridge, CO, USA, 2–8 February 2017.
12. Brugarolas, P. Guidance, Navigation and Control for the Entry, Descent, and Landing of the Mars 2020 Mission. In Proceedings of the 40th Annual Guidance and Control Conference, Breckenridge, CO, USA, 2–8 February 2017.
13. Shao, W.; Cao, L.; Guo, W.; Xie, J.; Gu, T. Visual Navigation Algorithm Based on Line Geomorphic Feature Matching for Mars Landing. *Acta Astronaut.* **2020**, *173*, 383–391. [CrossRef]
14. Nelessen, A.; Sackier, C.; Clark, I.; Brugarolas, P.; Villar, G.; Chen, A.; Stehura, A.; Otero, R.; Stilley, E.; Way, D. Mars 2020 Entry, Descent, and Landing System Overview. In Proceedings of the 2019 IEEE Aerospace Conference, Big Sky, MT, USA, 2–9 March 2019; Institute of Electrical and Electronics Engineers (IEEE): Piscataway, NJ, USA, 2019; pp. 1–20.
15. Johnson, A.E.; Aaron, S.B.; Ansari, H.; Bergh, C.; Bourdu, H.; Butler, J.; Chang, J.; Cheng, R.; Cheng, Y.; Clark, K. Mars 2020 Lander Vision System Flight Performance. In Proceedings of the AIAA SciTech 2022 Forum, San Diego, CA, USA, 3–7 January 2022; p. 1214.
16. Diniega, S.; Bramson, A.; Buratti, B.; Buhler, P.; Burr, D.; Chojnacki, M.; Conway, S.; Daubar, I.; Dinwiddie, C.L.; Galofre, A.G.; et al. Mars as a "Natural Laboratory" for Studying Surface Activity on a Range of Planetary Bodies. *Bull. Am. Astron. Soc.* **2021**, *53*, 123.
17. Diniega, S.; Bramson, A.M.; Buratti, B.; Buhler, P.; Burr, D.M.; Chojnacki, M.; Conway, S.J.; Dundas, C.M.; Hansen, C.J.; McEwen, A.S.; et al. Modern Mars' Geomorphological Activity, Driven by Wind, Frost, and Gravity. *Geomorphology* **2021**, *380*, 107627. [CrossRef]
18. Domagal-Goldman, S.D.; Wright, K.E.; Adamala, K.; de La Rubia, L.A.; Bond, J.; Dartnell, L.R.; Goldman, A.D.; Lynch, K.; Naud, M.-E.; Paulino-Lima, I.G.; et al. The Astrobiology Primer v2. 0. *Astrobiology* **2016**, *16*, 561.
19. Changela, H.G.; Chatzitheodoridis, E.; Antunes, A.; Beaty, D.; Bouw, K.; Bridges, J.C.; Capova, K.A.; Cockell, C.S.; Conley, C.A.; Dadachova, E.; et al. Mars: New Insights and Unresolved Questions. *Int. J. Astrobiol.* **2021**, *20*, 394–426. [CrossRef]
20. Maxwell, A.E.; Warner, T.A.; Fang, F. Implementation of Machine-Learning Classification in Remote Sensing: An Applied Review. *Int. J. Remote Sens.* **2018**, *39*, 2784–2817. [CrossRef]
21. Ferreira, B.; Iten, M.; Silva, R.G. Monitoring Sustainable Development by Means of Earth Observation Data and Machine Learning: A Review. *Environ. Sci. Eur.* **2020**, *32*, 120. [CrossRef]
22. Lary, D.J.; Zewdie, G.K.; Liu, X.; Wu, D.; Levetin, E.; Allee, R.J.; Malakar, N.; Walker, A.; Mussa, H.; Mannino, A.; et al. *Machine Learning Applications for Earth Observation*; Springer: Cham, Switzerland, 2018; ISBN 9783319656328.
23. Salcedo-Sanz, S.; Ghamisi, P.; Piles, M.; Werner, M.; Cuadra, L.; Moreno-Martínez, A.; Izquierdo-Verdiguier, E.; Muñoz-Marí, J.; Mosavi, A.; Camps-Valls, G. Machine Learning Information Fusion in Earth Observation: A Comprehensive Review of Methods, Applications and Data Sources. *Inf. Fusion* **2020**, *63*, 256–272. [CrossRef]

24. Vali, A.; Comai, S.; Matteucci, M. Deep Learning for Land Use and Land Cover Classification Based on Hyperspectral and Multispectral Earth Observation Data: A Review. *Remote Sens.* **2020**, *12*, 2495. [CrossRef]
25. Hoeser, T.; Kuenzer, C. Object Detection and Image Segmentation with Deep Learning on Earth Observation Data: A Review-Part I: Evolution and Recent Trends. *Remote Sens.* **2020**, *12*, 1667. [CrossRef]
26. Pandey, P.C.; Koutsias, N.; Petropoulos, G.P.; Srivastava, P.K.; ben Dor, E. Land Use/Land Cover in View of Earth Observation: Data Sources, Input Dimensions, and Classifiers—A Review of the State of the Art. *Geocarto Int.* **2021**, *36*, 957–988. [CrossRef]
27. Selva, D.; Krejci, D. A Survey and Assessment of the Capabilities of Cubesats for Earth Observation. *Acta Astron.* **2012**, *74*, 50–68. [CrossRef]
28. Secades, C.; O'Connor, B.; Brown, C.; Walpole, M.; Skidmore, A.; Wang, T.; Groen, T.A.; Herkt, K.M.B.; Niamir, A. Earth observation for biodiversity monitoring, Canadian Electronic Library. Available online: https://policycommons.net/artifacts/1189083/earth-observation-for-biodiversity-monitoring/1742209/ (accessed on 8 June 2022).
29. Merchant, C.J.; Paul, F.; Popp, T.; Ablain, M.; Bontemps, S.; Defourny, P.; Hollmann, R.; Lavergne, T.; Laeng, A.; de Leeuw, G. Uncertainty Information in Climate Data Records from Earth Observation. *Earth Syst. Sci. Data* **2017**, *9*, 511–527. [CrossRef]
30. Chuvieco, E.; Mouillot, F.; van der Werf, G.R.; San Miguel, J.; Tanase, M.; Koutsias, N.; García, M.; Yebra, M.; Padilla, M.; Gitas, I. Historical Background and Current Developments for Mapping Burned Area from Satellite Earth Observation. *Remote Sens. Environ.* **2019**, *225*, 45–64. [CrossRef]
31. Ouma, Y.O. Advancements in Medium and High Resolution Earth Observation for Land-Surface Imaging: Evolutions, Future Trends and Contributions to Sustainable Development. *Adv. Space Res.* **2016**, *57*, 110–126. [CrossRef]
32. Richter, K.; Hank, T.B.; Mauser, W.; Atzberger, C. Derivation of Biophysical Variables from Earth Observation Data: Validation and Statistical Measures. *J. Appl. Remote Sens.* **2012**, *6*, 63557. [CrossRef]
33. Pfeifer, M.; Disney, M.; Quaife, T.; Marchant, R. Terrestrial Ecosystems from Space: A Review of Earth Observation Products for Macroecology Applications. *Glob. Ecol. Biogeogr.* **2012**, *21*, 603–624. [CrossRef]
34. Kansakar, P.; Hossain, F. A Review of Applications of Satellite Earth Observation Data for Global Societal Benefit and Stewardship of Planet Earth. *Space Policy* **2016**, *36*, 46–54. [CrossRef]
35. Hirschmugl, M.; Gallaun, H.; Dees, M.; Datta, P.; Deutscher, J.; Koutsias, N.; Schardt, M. Methods for Mapping Forest Disturbance and Degradation from Optical Earth Observation Data: A Review. *Curr. For. Rep.* **2017**, *3*, 32–45. [CrossRef]
36. Li, D.; Shan, J.; Gong, J. *Geospatial Technology for Earth Observation*; Springer Science & Business Media: Berlin/Heidelberg, Germany, 2009; ISBN 1441900500.
37. Sąsiadek, J. Space Robotics and Its Challenges. In *Aerospace Robotics*; Springer: Berlin/Heidelberg, Germany, 2013; pp. 1–8.
38. Lumia, R.; Albus, J.S. Teleoperation and Autonomy for Space Robotics. *Robot. Auton. Syst.* **1988**, *4*, 27–33. [CrossRef]
39. Hambuchen, K.A.; Roman, M.C.; Sivak, A.; Herblet, A.; Koenig, N.; Newmyer, D.; Ambrose, R. NASA's Space Robotics Challenge: Advancing Robotics for Future Exploration Missions. In Proceedings of the AIAA SPACE and Astronautics Forum and Exposition, Orlando, FL, USA, 12–14 September 2017; p. 5120.
40. Meshka, L. Risk Considerations for Autonomy Software. In Proceedings of the 2020 Annual Reliability and Maintainability Symposium (RAMS), Palm Springs, CA, USA, 27–30 January 2020; Institute of Electrical and Electronics Engineers (IEEE): Piscataway, NJ, USA, 2020; pp. 1–6.
41. Gao, Y.; Chien, S. Review on Space Robotics: Toward Top-Level Science through Space Exploration. *Sci. Robot.* **2017**, *2*, eaan5074. [CrossRef]
42. Olivares-Alarcos, A.; Beßler, D.; Khamis, A.; Goncalves, P.; Habib, M.K.; Bermejo-Alonso, J.; Barreto, M.; Diab, M.; Rosell, J.; Quintas, J. A Review and Comparison of Ontology-Based Approaches to Robot Autonomy. *Knowl. Eng. Rev.* **2019**, *34*, e29. [CrossRef]
43. Read, N.; Woods, M.; Karachalios, S. Novelty or Anomaly Hunter–Driving Next Generation Science Autonomy With Large High Quality Dataset Collection. In Proceedings of the ESA AI and Robotics at i-SAIRAS 2020, Virtual, 19–23 October 2020.
44. Volpe, R. Rover Functional Autonomy Development for the Mars Mobile Science Laboratory. In Proceedings of the 2003 IEEE Aerospace Conference, Big Sky, MT, USA, 8–15 March 2003; Volume 2, pp. 643–652.
45. Volpe, R. Rover Technology Development and Mission Infusion beyond MER. In Proceedings of the 2005 IEEE Aerospace Conference, Big Sky, MT, USA, 5–12 March 2005; Institute of Electrical and Electronics Engineers (IEEE): Piscataway, NJ, USA, 2005; pp. 971–981.
46. Munoz, P.; R-Moreno, M.D.; Martınez, A. A First Approach for the Autonomy of the Exomars Rover Using a 3-Tier Architecture. In Proceedings of the 11th ESA Symposium on Advanced Space Technologies for Robotics and Automation, Noordwijk, The Netherlands, 14 April 2011.
47. Shaukat, A.; Blacker, P.C.; Spiteri, C.; Gao, Y. Towards Camera-LIDAR Fusion-Based Terrain Modelling for Planetary Surfaces: Review and Analysis. *Sensors* **2016**, *16*, 1952. [CrossRef]
48. Schenker, P.S.; Huntsberger, T.L.; Pirjanian, P.; Baumgartner, E.T.; Tunstel, E. Planetary Rover Developments Supporting Mars Exploration, Sample Return and Future Human-Robotic Colonization. *Auton. Robot.* **2003**, *14*, 103–126. [CrossRef]
49. Nesnas, I.A.D.; Fesq, L.M.; Volpe, R.A. Autonomy for Space Robots: Past, Present, and Future. *Curr. Robot. Rep.* **2021**, *2*, 251–263. [CrossRef]
50. Woods, M.; Shaw, A.; Barnes, D.; Price, D.; Long, D.; Pullan, D. Autonomous Science for an ExoMars Rover–like Mission. *J. Field Robot.* **2009**, *26*, 358–390. [CrossRef]

51. Rybus, T. Obstacle Avoidance in Space Robotics: Review of Major Challenges and Proposed Solutions. *Prog. Aerosp. Sci.* **2018**, *101*, 31–48. [CrossRef]
52. Jasiobedzki, P.; Anders, C. Computer Vision for Space Robotics: Applications, Role and Performance. *IFAC Proc. Vol.* **1998**, *31*, 95–102. [CrossRef]
53. Rabideau, G.; Benowitz, E. Prototyping an Onboard Scheduler for the Mars 2020 Rover. In Proceedings of the 10th International Workshop on Planning and Scheduling for Space (IWPSS 2017), Pittsburgh, PA, USA, 15–17 June 2017.
54. Daftry, S.; Abcouwer, N.; del Sesto, T.; Venkatraman, S.; Song, J.; Igel, L.; Byon, A.; Rosolia, U.; Yue, Y.; Ono, M. MLNav: Learning to Safely Navigate on Martian Terrains. *IEEE Robot. Autom. Lett.* **2022**, *7*, 5461–5468. [CrossRef]
55. Russell, S.; Norvig, P. *Artificial Intelligence: A Modern Approach*; Pearson: London, UK, 2002.
56. Bishop, C.M.; Nasrabadi, N.M. *Pattern Recognition and Machine Learning*; Springer: New York, NY, USA, 2006; Volume 4.
57. Jordan, M.I.; Mitchell, T.M. Machine Learning: Trends, Perspectives, and Prospects. *Science* **2015**, *349*, 255–260. [CrossRef]
58. Ayodele, T.O. Types of Machine Learning Algorithms. *New Adv. Mach. Learn.* **2010**, *3*, 19–48.
59. Ray, S. A Quick Review of Machine Learning Algorithms. In Proceedings of the 2019 International conference on machine learning, big data, cloud and parallel computing (COMITCon), Faridabad, India, 14–16 February 2019; Institute of Electrical and Electronics Engineers (IEEE): Piscataway, NJ, USA, 2019; pp. 35–39.
60. Zhuang, F.; Qi, Z.; Duan, K.; Xi, D.; Zhu, Y.; Zhu, H.; Xiong, H.; He, Q. A Comprehensive Survey on Transfer Learning. *Proc. IEEE* **2020**, *109*, 43–76. [CrossRef]
61. Day, O.; Khoshgoftaar, T.M. A Survey on Heterogeneous Transfer Learning. *J. Big Data* **2017**, *4*, 1–42. [CrossRef]
62. Tan, C.; Sun, F.; Kong, T.; Zhang, W.; Yang, C.; Liu, C. A Survey on Deep Transfer Learning. In Proceedings of the International Conference on Artificial Neural Networks, Rhodes, Greece, 4–7 October 2018; Springer: Berling, Germany, 2018; pp. 270–279.
63. Bozinovski, S. Reminder of the First Paper on Transfer Learning in Neural Networks, 1976. *Informatica* **2020**, *44*. [CrossRef]
64. Kaboli, M. A Review of Transfer Learning Algorithms. [Research Report] Technische Universität München. 2017. hal-01575126. Available online: https://hal.archives-ouvertes.fr/hal-01575126 (accessed on 8 June 2022).
65. Krizhevsky, A.; Sutskever, I.; Hinton, G.E. ImageNet Classification with Deep Convolutional Neural Networks. *Commun. ACM* **2017**, *60*, 84–90. [CrossRef]
66. Lin, T.-Y.; Goyal, P.; Girshick, R.; He, K.; Dollár, P. Focal Loss for Dense Object Detection. In Proceedings of the IEEE International Conference on Computer Vision, Venice, Italy, 22–29 October 2017; pp. 2980–2988.
67. He, K.; Gkioxari, G.; Dollár, P.; Girshick, R. Mask R-Cnn. In Proceedings of the IEEE International Conference on Computer Vision, Venice, Italy, 22–29 October 2017; pp. 2961–2969.
68. Iandola, F.N.; Han, S.; Moskewicz, M.W.; Ashraf, K.; Dally, W.J.; Keutzer, K. SqueezeNet: AlexNet-Level Accuracy with 50x Fewer Parameters and <0.5 MB Model Size. *arXiv* **2016**, arXiv:1602.07360.
69. He, K.; Zhang, X.; Ren, S.; Sun, J. Deep Residual Learning for Image Recognition. In Proceedings of the IEEE Conference on Computer Vision and Pattern Recognition, Las Vegas, NV, USA, 27–30 June 2016; pp. 770–778.
70. Mikolov, T.; Le, Q.V.; Sutskever, I. Exploiting Similarities among Languages for Machine Translation. *arXiv* **2013**, arXiv:1309.4168.
71. Pennington, J.; Socher, R.; Manning, C.D. Glove: Global Vectors for Word Representation. In Proceedings of the 2014 Conference on Empirical Methods in Natural Language Processing (EMNLP), Doha, Qatar, 25–29 October 2014; pp. 1532–1543.
72. Szegedy, C.; Liu, W.; Jia, Y.; Sermanet, P.; Reed, S.; Anguelov, D.; Erhan, D.; Vanhoucke, V.; Rabinovich, A. Going Deeper with Convolutions. In Proceedings of the IEEE Conference on Computer Vision and Pattern Recognition, Boston, MA, USA, 7–12 June 2015; pp. 1–9.
73. Zhang, X.; Zou, J.; He, K.; Sun, J. Accelerating very Deep Convolutional Networks for Classification and Detection. *IEEE Trans. Pattern Anal. Mach. Intell.* **2016**, *38*, 1943–1955. [CrossRef] [PubMed]
74. Li, Y.; Hou, X.; Koch, C.; Rehg, J.M.; Yuille, A.L. The Secrets of Salient Object Segmentation. In Proceedings of the IEEE Conference on Computer Vision and Pattern Recognition, Columbus, OH, USA, 23–28 June 2014; pp. 280–287.
75. Movahedi, V.; Elder, J.H. Design and Perceptual Validation of Performance Measures for Salient Object Segmentation. In Proceedings of the 2010 IEEE Computer Society Conference on Computer Vision and Pattern Recognition-Workshops, San Francisco, CA, USA, 13–18 June 2010; Institute of Electrical and Electronics Engineers (IEEE): Piscataway, NJ, USA, 2010; pp. 49–56.
76. Chien, S.-Y.; Ma, S.-Y.; Chen, L.-G. Efficient Moving Object Segmentation Algorithm Using Background Registration Technique. *IEEE Trans. Circuits Syst. Video Technol.* **2002**, *12*, 577–586. [CrossRef]
77. Wang, T.; Zhang, X.; Sun, J. Implicit Feature Pyramid Network for Object Detection. *arXiv* **2020**, arXiv:2012.13563.
78. Kim, S.-W.; Kook, H.-K.; Sun, J.-Y.; Kang, M.-C.; Ko, S.-J. Parallel Feature Pyramid Network for Object Detection. In Proceedings of the European Conference on Computer Vision (ECCV), Munich, Germany, 8–14 September 2018; pp. 234–250.
79. Lin, T.-Y.; Dollár, P.; Girshick, R.; He, K.; Hariharan, B.; Belongie, S. Feature Pyramid Networks for Object Detection. In Proceedings of the IEEE Conference on Computer Vision and Pattern Recognition, Honolulu, HI, USA, 21–26 June 2017; pp. 2117–2125.
80. Deng, C.; Wang, M.; Liu, L.; Liu, Y.; Jiang, Y. Extended Feature Pyramid Network for Small Object Detection. *IEEE Trans. Multimed.* **2021**, *24*, 1968–1979. [CrossRef]
81. Zhao, Y.; Han, R.; Rao, Y. A New Feature Pyramid Network for Object Detection. In Proceedings of the 2019 International Conference on Virtual Reality and Intelligent Systems (ICVRIS), Jishou, China, 14–15 September 2019; Institute of Electrical and Electronics Engineers (IEEE): Piscataway, NJ, USA, 2019; pp. 428–431.

82. Bland, P. Crater Counting. *Astron. Geophys.* **2003**, *44*, 4–21. [CrossRef]
83. Öpik, E.J. Cratering and the Moon's Surface. In *Advances in Astronomy and Astrophysics*; Elsevier: Amsterdam, The Netherlands, 1971; Volume 8, pp. 107–337. ISBN 0065-2180.
84. Tyrie, A. Age Dating of Mare in the Lunar Crater Tsiolkovsky by Crater-Counting Method. *Earth Moon Planets* **1988**, *42*, 245–264. [CrossRef]
85. Neukum, G.; König, B.; Fechtig, H.; Storzer, D. Cratering in the Earth-Moon System-Consequences for Age Determination by Crater Counting. In Proceedings of the Lunar and Planetary Science Conference, Houston, TX, USA, 17–21 March 1975; Volume 6, pp. 2597–2620.
86. Neukum, G.; Wise, D.U. Mars: A Standard Crater Curve and Possible New Time Scale: Cratering Links to Lunar Time Suggest That Mars Died Long Ago. *Science* **1976**, *194*, 1381–1387. [CrossRef]
87. Baldwin, R.B. Mars: An Estimate of the Age of Its Surface. *Science* **1965**, *149*, 1498–1499. [CrossRef]
88. Yang, S.; Cai, Z. High-Resolution Feature Pyramid Network for Automatic Crater Detection on Mars. *IEEE Trans. Geosci. Remote Sens.* **2022**, *60*, 4601012. [CrossRef]
89. Jin, S.; Zhang, T. Automatic Detection of Impact Craters on Mars Using a Modified Adaboosting Method. *Planet. Space Sci.* **2014**, *99*, 112–117. [CrossRef]
90. Stepinski, T.F.; Ding, W.; Vilalta, R. Detecting Impact Craters in Planetary Images Using Machine Learning. In *Intelligent Data Analysis for Real-Life Applications: Theory and Practice*; IGI Global: Hershey, PA, USA, 2012; pp. 146–159.
91. DeLatte, D.M.; Crites, S.T.; Guttenberg, N.; Tasker, E.J.; Yairi, T. Segmentation Convolutional Neural Networks for Automatic Crater Detection on Mars. *IEEE J. Sel. Top. Appl. Earth Obs. Remote Sens.* **2019**, *12*, 2944–2957. [CrossRef]
92. Hsu, C.Y.; Li, W.; Wang, S. Knowledge-Driven Geoai: Integrating Spatial Knowledge into Multi-Scale Deep Learning for Mars Crater Detection. *Remote Sens.* **2021**, *13*, 2116. [CrossRef]
93. AlMarzooqi, M.; AlNaqbi, A.; AlMheiri, A.; Bezawada, S.; Mohamed, E.A.; Zaki, N. Increase the Exploitation of Mars Satellite Images Via Deep Learning Techniques. In Proceedings of the 2018 International Conference on Robotics, Control and Automation Engineering, Beijing, China, 26–28 December 2018; Association for Computing Machinery: New York, NY, USA, 2018; pp. 171–175.
94. Stepinski, T.F.; Mendenhall, M.P.; Bue, B.D. Machine Cataloging of Impact Craters on Mars. *Icarus* **2009**, *203*, 77–87. [CrossRef]
95. Lee, C. Automated Crater Detection on Mars Using Deep Learning. *Planet. Space Sci.* **2019**, *170*, 16–28. [CrossRef]
96. Plesko, C.; Brumby, S.; Asphaug, E.; Chamberlain, D.; Engel, T. Automatic Crater Counts on Mars. *Lunar Planet. Inst. Conf. Abstr.* **2004**, *35*, 1935.
97. Vinogradova, T.; Burl, M.; Mjolsness, E. Training of a Crater Detection Algorithm for Mars Crater Imagery. In Proceedings of the IEEE Aerospace Conference, Big Sky, MT, USA, 9–16 March 2002; Institute of Electrical and Electronics Engineers (IEEE): Piscataway, NJ, USA, 2002; Volume 7, p. 7.
98. DeLatte, D.M.; Crites, S.T.; Guttenberg, N.; Tasker, E.J.; Yairi, T. Exploration of Machine Learning Methods for Crater Counting on Mars. In Proceedings of the 49th Lunar and Planetary Science Conference 2018, The Woodlands, TX, USA, 19–23 March 2018; Volume 49.
99. Bouley, S.; Craddock, R.A.; Mangold, N.; Ansan, V. Comparison of Different Crater Counting Methods Applicated to Parana Valles. In Proceedings of the 40th Annual Lunar and Planetary Science Conference, The Woodlands, TX, USA, 21–25 March 2016; p. 1097.
100. Werner, S.C.; Tanaka, K.L.; Skinner Jr, J.A. Mars: The Evolutionary History of the Northern Lowlands Based on Crater Counting and Geologic Mapping. *Planet. Space Sci.* **2011**, *59*, 1143–1165. [CrossRef]
101. Lagain, A.; Servis, K.; Benedix, G.K.; Norman, C.; Anderson, S.; Bland, P.A. Model Age Derivation of Large Martian Impact Craters, Using Automatic Crater Counting Methods. *Earth Space Sci.* **2021**, *8*, e2020EA001598. [CrossRef]
102. Di, K.; Li, W.; Yue, Z.; Sun, Y.; Liu, Y. A Machine Learning Approach to Crater Detection from Topographic Data. *Adv. Space Res.* **2014**, *54*, 2419–2429. [CrossRef]
103. Christoff, N.; Jorda, L.; Viseur, S.; Bouley, S.; Manolova, A.; Mari, J.-L. Automated Extraction of Crater Rims on 3D Meshes Combining Artificial Neural Network and Discrete Curvature Labeling. *Earth Moon Planets* **2020**, *124*, 51–72. [CrossRef]
104. Benedix, G.K.; Lagain, A.; Chai, K.; Meka, S.; Anderson, S.; Norman, C.; Bland, P.A.; Paxman, J.; Towner, M.C.; Tan, T. Deriving Surface Ages on Mars Using Automated Crater Counting. *Earth Space Sci.* **2020**, *7*, e2019EA001005. [CrossRef]
105. Gao, A.; Daubar, I.J.; Wexler, D.; Wagstaff, K.L.; Bickel, V.; Doran, G. Using Machine Learning to Complement New Martial Crater Inventories. In Proceedings of the 52nd Lunar and Planetary Science Conference, Virtual, 15–19 March 2021.
106. Hartmann, W.K. Martian Cratering 8: Isochron Refinement and the Chronology of Mars. *Icarus* **2005**, *174*, 294–320. [CrossRef]
107. Xiao, Z.; Strom, R.G. Problems Determining Relative and Absolute Ages Using the Small Crater Population. *Icarus* **2012**, *220*, 254–267. [CrossRef]
108. Robbins, S.J.; Hynek, B.M.; Lillis, R.J.; Bottke, W.F. Large Impact Crater Histories of Mars: The Effect of Different Model Crater Age Techniques. *Icarus* **2013**, *225*, 173–184. [CrossRef]
109. Edwards, C.S.; Nowicki, K.J.; Christensen, P.R.; Hill, J.; Gorelick, N.; Murray, K. Mosaicking of Global Planetary Image Datasets: 1. Techniques and Data Processing for Thermal Emission Imaging System (THEMIS) Multi-spectral Data. *J. Geophys. Res. Planets* **2011**, *116*. [CrossRef]
110. Albee, A.L.; Arvidson, R.E.; Palluconi, F.; Thorpe, T. Overview of the Mars Global Surveyor Mission. *J. Geophys. Res. Planets* **2001**, *106*, 23291–23316. [CrossRef]

111. De, K.; Ruj, T.; Kundu, A.; Dasgupta, N.; Kawai, K. Evolution of Pyrrhae Fossae, Mars: An Explication from the Age Estimation Using the Buffered Crater Counting Technique. *Curr. Sci.* **2021**, *121*, 906. [CrossRef]
112. Fassett, C.I.; Head, J.W., III. The Timing of Martian Valley Network Activity: Constraints from Buffered Crater Counting. *Icarus* **2008**, *195*, 61–89. [CrossRef]
113. Fergason, R.L.; Hare, T.M.; Laura, J. *HRSC and MOLA Blended Digital Elevation Model at 200m V2*; Astrogeology PDS Annex, US Geological Survey; USGS Astrogeology Science Center: Flagstaff, AZ, USA, 2018.
114. Li, G.; Geng, Y.; Xiao, X. Multi-Scale Rock Detection on Mars. *Sci. China Inf. Sci.* **2018**, *61*, 102301. [CrossRef]
115. Pan, L.; Gui, C.; Barnes, D.; Shang, C. Mars Multispectral Image Classification Using Machine Learning Techniques. In Proceedings of the Thirty-First Annual Conference on Innovative Applications of Artificial Intelligence, Honolulu, HI, USA, 28–30 January 2013.
116. Shang, C.; Barnes, D. Fuzzy-Rough Feature Selection Aided Support Vector Machines for Mars Image Classification. *Comput. Vis. Image Underst.* **2013**, *117*, 202–213. [CrossRef]
117. Rashno, A.; Nazari, B.; Sadri, S.; Saraee, M. Effective Pixel Classification of Mars Images Based on Ant Colony Optimization Feature Selection and Extreme Learning Machine. *Neurocomputing* **2017**, *226*, 66–79. [CrossRef]
118. Haq, A.U.; Leitner, J.; Harding, S.; Forster, A.; Schmidhuber, J. Mars Terrain Image Classification Using Cartesian Genetic Programming. In Proceedings of the 11th International Symposium on Artificial Intelligence, Robotics and Automation in Space, i-SAIRAS 2012, Turin, Italy, 4–6 September 2012; European Space Agency (ESA): Paris, France, 2012; pp. 1–8.
119. Rothrock, B.; Papon, J.; Kennedy, R.; Ono, M.; Heverly, M.; Cunningham, C. SPOC: Deep Learning-Based Terrain Classification for Mars Rover Missions. In Proceedings of the AIAA Space and Astronautics Forum and Exposition, SPACE 2016, Long Beach, CA, USA, 13–16 September 2016; pp. 1–12. [CrossRef]
120. Chakravarthy, A.S.; Roy, R.; Ravirathinam, P. MRSCAtt: A Spatio-Channel Attention-Guided Network for Mars Rover Image Classification. In Proceedings of the IEEE Computer Society Conference on Computer Vision and Pattern Recognition Workshops 2021, Nashville, TN, USA, 19–25 June 2021; pp. 1961–1970. [CrossRef]
121. Shang, C.; Barnes, D.; Shen, Q. Facilitating Efficient Mars Terrain Image Classification with Fuzzy-Rough Feature Selection. *Int. J. Hybrid Intell. Syst.* **2011**, *8*, 3–13. [CrossRef]
122. Huang, G.; Yang, L.; Cai, Y.; Zhang, D. Terrain Classification-Based Rover Traverse Planner with Kinematic Constraints for Mars Exploration. *Planet. Space Sci.* **2021**, *209*, 105371. [CrossRef]
123. Hu, S.; Liu, J.; Kang, Z. DeepLabV3+/Efficientnet Hybrid Network-Based Scene Area Judgment for the Mars Unmanned Vehicle System. *Sensors* **2021**, *21*, 8136. [CrossRef] [PubMed]
124. Ogohara, K.; Gichu, R. Automated Segmentation of Textured Dust Storms on Mars Remote Sensing Images Using an Encoder-Decoder Type Convolutional Neural Network. *Comput. Geosci.* **2022**, *160*, 105043. [CrossRef]
125. Gichu, R.; Ogohara, K. Segmentation of Dust Storm Areas on Mars Images Using Principal Component Analysis and Neural Network. *Prog. Earth Planet. Sci.* **2019**, *6*, 19. [CrossRef]
126. Sakimoto, S.E.H.; Lewis, D.D.; Dileep, S.; Memon, P.; Beveridge, J.R.; Blanchard, N.T.; Gregg, T.K.P.; Carley, T.L.; Azari, A.; Biersteker, J.B.; et al. Deep Learning for an Inventory of Small to Midsize Volcanic Edifices on Mars. In Proceedings of the Lunar and Planetary Science Conference, Virtual, 15–19 March 2021; Volume 53, p. 1626.
127. Palafox, L.F.; Hamilton, C.W.; Scheidt, S.P.; Alvarez, A.M. Automated Detection of Geological Landforms on Mars Using Convolutional Neural Networks. *Comput. Geosci.* **2017**, *101*, 48–56. [CrossRef]
128. Bue, B.; Wagstaff, K.; Stillman, D. Automated Mapping and Characterization of RSL from HiRISE Data with MAARSL. In Proceedings of the AAS/Division for Planetary Sciences Meeting Abstracts# 49, Provo, Utah, 15–20 October 2017; Volume 49, pp. 400–402.
129. Tao, Y.; Muller, J.-P. Automated Dynamic Feature Tracking of RSLs on the Martian Surface through HiRISE Super-Resolution Restoration and 3D Reconstruction Techniques. *Eur. Planet. Sci. Congr.* **2017**, *11*, 774. [CrossRef]
130. Tao, Y.; Muller, J.-P. Automated Feature Detection and Tracking of RSLs at Valles Marineris through Super-Resolution Restoration and Deep Learning Using HiRISE Images and 3D Terrain Models. In Proceedings of the European Planetary Science Congress, Berlin, Germany, 16–21 September 2018; p. EPSC2018-509.
131. Fanara, L.; Gwinner, K.; Hauber, E.; Oberst, J. Automated Detection of Block Falls in the North Polar Region of Mars. *Planet. Space Sci.* **2020**, *180*, 104733. [CrossRef]
132. Bickel, V.T.; Conway, S.J.; Tesson, P.-A.; Manconi, A.; Loew, S.; Mall, U. Deep Learning-Driven Detection and Mapping of Rockfalls on Mars. *IEEE J. Sel. Top. Appl. Earth Obs. Remote Sens.* **2020**, *13*, 2831–2841. [CrossRef]
133. Nagle-Mcnaughton, T.; McClanahan, T.; Scuderi, L. PlaNet: A Neural Network for Detecting Transverse Aeolian Ridges on Mars. *Remote Sens.* **2020**, *12*, 3607. [CrossRef]
134. Rubanenko, L.; Perez-Lopez, S.; Schull, J.; Lapotre, M.G.A. Automatic Detection and Segmentation of Barchan Dunes on Mars and Earth Using a Convolutional Neural Network. *IEEE J. Sel. Top. Appl. Earth Obs. Remote Sens.* **2021**, *14*, 9364–9371. [CrossRef]
135. Wagstaff, K.L.; Lu, Y.; Stanboli, A.; Grimes, K.; Gowda, T.; Padams, J. Deep Mars: CNN Classification of Mars Imagery for the PDS Imaging Atlas. In Proceedings of the 32nd AAAI Conference on Artificial Intelligence, AAAI 2018, New Orleans, LA, USA, 2–7 February 2018; pp. 7867–7872.

136. Barrett, A.M.; Balme, M.R.; Woods, M.; Karachalios, S.; Petrocelli, D.; Joudrier, L.; Sefton-Nash, E. NOAH-H, a Deep-Learning, Terrain Classification System for Mars: Results for the ExoMars Rover Candidate Landing Sites. *Icarus* **2022**, *371*, 114701. [CrossRef]
137. Wilhelm, T.; Geis, M.; Püttschneider, J.; Sievernich, T.; Weber, T.; Wohlfarth, K.; Wöhler, C. DoMars16k: A Diverse Dataset for Weakly Supervised Geomorphologic Analysis on Mars. *Remote Sens.* **2020**, *12*, 3981. [CrossRef]
138. Gupta, V.; Gupta, S.K.; Kim, J. Automated Discontinuity Detection and Reconstruction in Subsurface Environment of Mars Using Deep Learning: A Case Study of SHARAD Observation. *Appl. Sci.* **2020**, *10*, 2279. [CrossRef]
139. Sun, C.; Xu, W.; Tan, Y.; Zhang, Y.; Yue, Z.; Zou, L.; Shabbir, S.; Wu, M.; Chen, F.; Yu, J. From Machine Learning to Transfer Learning in Laser-Induced Breakdown Spectroscopy Analysis of Rocks for Mars Exploration. *Sci. Rep.* **2021**, *11*, 21379. [CrossRef]
140. Fabre, C.; Maurice, S.; Wiens, R.; Sautter, V. ChemCam LIBS Instrument: Complete Characterization of the Onboard Calibration Silicate Targets (MSL Rover). In Proceedings of the 41st Lunar and Planetary Science Conference, The Woodlands, TX, USA, 1–5 March 2010; Volume 1533, p. 1835.
141. Wiens, R.C.; Maurice, S.; Barraclough, B.; Saccoccio, M.; Barkley, W.C.; Bell, J.F.; Bender, S.; Bernardin, J.; Blaney, D.; Blank, J. The ChemCam Instrument Suite on the Mars Science Laboratory (MSL) Rover: Body Unit and Combined System Tests. *Space Sci. Rev.* **2012**, *170*, 167–227. [CrossRef]
142. Clegg, S.M.; Wiens, R.C.; Anderson, R.; Forni, O.; Frydenvang, J.; Lasue, J.; Cousin, A.; Payre, V.; Boucher, T.; Dyar, M.D. Recalibration of the Mars Science Laboratory ChemCam Instrument with an Expanded Geochemical Database. *Spectrochim. Acta Part B At. Spectrosc.* **2017**, *129*, 64–85. [CrossRef]
143. Wiens, R.C.; Maurice, S.; Lasue, J.; Forni, O.; Anderson, R.B.; Clegg, S.; Bender, S.; Blaney, D.; Barraclough, B.L.; Cousin, A. Pre-Flight Calibration and Initial Data Processing for the ChemCam Laser-Induced Breakdown Spectroscopy Instrument on the Mars Science Laboratory Rover. *Spectrochim. Acta Part B At. Spectrosc.* **2013**, *82*, 1–27. [CrossRef]
144. Agarwal, S.; Tosi, N.; Kessel, P.; Padovan, S.; Breuer, D.; Montavon, G. Toward Constraining Mars' Thermal Evolution Using Machine Learning. *Earth Space Sci.* **2021**, *8*, 1–26. [CrossRef]
145. Agarwal, S.; Tosi, N.; Breuer, D.; Padovan, S.; Kessel, P.; Montavon, G. A Machine-Learning-Based Surrogate Model of Mars' Thermal Evolution. *Geophys. J. Int.* **2020**, *222*, 1656–1670. [CrossRef]
146. Ruhunusiri, S.; Halekas, J.S.; Espley, J.R.; Eparvier, F.; Brain, D.; Mazelle, C.; Harada, Y.; DiBraccio, G.A.; Dong, Y.; Ma, Y.; et al. An Artificial Neural Network for Inferring Solar Wind Proxies at Mars. *Geophys. Res. Lett.* **2018**, *45*, 10855–10865. [CrossRef]
147. Celebi, M.E.; Aydin, K. *Unsupervised Learning Algorithms*; Springer: Berlin, Germany, 2016; ISBN 3319242113.
148. Kataria, A.; Singh, M.D. A Review of Data Classification Using K-Nearest Neighbour Algorithm. *Int. J. Emerg. Technol. Adv. Eng.* **2013**, *3*, 354–360.
149. Triguero, I.; García-Gil, D.; Maillo, J.; Luengo, J.; García, S.; Herrera, F. Transforming Big Data into Smart Data: An Insight on the Use of the K-nearest Neighbors Algorithm to Obtain Quality Data. *Wiley Interdiscip. Rev. Data Min. Knowl. Discov.* **2019**, *9*, e1289. [CrossRef]
150. Guo, G.; Wang, H.; Bell, D.; Bi, Y.; Greer, K. KNN Model-Based Approach in Classification. In Proceedings of the OTM Confederated International Conferences "On the Move to Meaningful Internet Systems", Sicily, Italy, 3–7 November 2003; Springer: New York, NY, USA, 2003; pp. 986–996.
151. Deng, Z.; Zhu, X.; Cheng, D.; Zong, M.; Zhang, S. Efficient KNN Classification Algorithm for Big Data. *Neurocomputing* **2016**, *195*, 143–148. [CrossRef]
152. Kohonen, T. The Self-Organizing Map. *Proc. IEEE* **1990**, *78*, 1464–1480. [CrossRef]
153. Kohonen, T. Essentials of the Self-Organizing Map. *Neural Netw.* **2013**, *37*, 52–65. [CrossRef]
154. Hsu, C.C. Generalizing Self-Organizing Map for Categorical Data. *IEEE Trans. Neural Netw.* **2006**, *17*, 294–304. [CrossRef]
155. Kohonen, T. Exploration of Very Large Databases by Self-Organizing Maps. In Proceedings of the IEEE International Conference on Neural Networks, Houston, TX, USA, 12 June 1997. [CrossRef]
156. McLachlan, G.J.; Lee, S.X.; Rathnayake, S.I. Finite Mixture Models. *Annu. Rev. Stat. Appl.* **2019**, *6*, 355–378. [CrossRef]
157. Melnykov, V.; Maitra, R. Finite Mixture Models and Model-Based Clustering. *Stat. Surv.* **2010**, *4*, 80–116. [CrossRef]
158. Young, D.S. An Overview of Mixture Models. *arXiv* **2008**, arXiv:0808.0383.
159. Plataniotis, K.N.; Hatzinakos, D. Gaussian Mixtures and Their Applications to Signal Processing. In *Advanced Signal Processing Handbook*; CRC Press: Boca Raton, FL, USA, 2017; pp. 89–124.
160. Roweis, S.; Ghahramani, Z. A Unifying Review of Linear Gaussian Models. *Neural Comput.* **1999**, *11*, 305–345. [CrossRef] [PubMed]
161. Fonseca, J.R.S.; Cardoso, M.G.M.S. Mixture-Model Cluster Analysis Using Information Theoretical Criteria. *Intell. Data Anal.* **2007**, *11*, 155–173. [CrossRef]
162. Zong, B.; Song, Q.; Min, M.R.; Cheng, W.; Lumezanu, C.; Cho, D.; Chen, H. Deep Autoencoding Gaussian Mixture Model for Unsupervised Anomaly Detection. In Proceedings of the International Conference on Learning Representations, Vancouver, BC, Canada, 30 April–3 May 2018.
163. McLachlan, G.J.; Rathnayake, S. On the Number of Components in a Gaussian Mixture Model. *Wiley Interdisc. Rev. Data Min. Knowl. Discov.* **2014**, *4*, 341–355. [CrossRef]
164. Leung, K.; Leckie, C. Unsupervised Anomaly Detection in Network Intrusion Detection Using Clusters. In Proceedings of the Twenty-eighth Australasian conference on Computer Science, Newcastle, Australia, 1 January 2005; Volume 38, pp. 333–342.

165. Goix, N. How to Evaluate the Quality of Unsupervised Anomaly Detection Algorithms? *arXiv* **2016**, arXiv:1607.01152.
166. Kiran, B.R.; Thomas, D.M.; Parakkal, R. An Overview of Deep Learning Based Methods for Unsupervised and Semi-Supervised Anomaly Detection in Videos. *J. Imaging* **2018**, *4*, 36. [CrossRef]
167. Goldstein, M.; Uchida, S. A Comparative Evaluation of Unsupervised Anomaly Detection Algorithms for Multivariate Data. *PLoS ONE* **2016**, *11*, e0152173. [CrossRef]
168. Abdi, H.; Williams, L.J. Principal Component Analysis. *Wiley Interdisc. Rev. Comput. Stat.* **2010**, *2*, 433–459. [CrossRef]
169. Wold, S.; Esbensen, K.; Geladi, P. Principal Component Analysis. *Chemom. Intell. Lab. Syst.* **1987**, *2*, 37–52. [CrossRef]
170. Tipping, M.E.; Bishop, C.M. Probabilistic Principal Component Analysis. *J. R. Stat. Soc. Ser. B* **1999**, *61*, 611–622. [CrossRef]
171. Bro, R.; Smilde, A.K. Principal Component Analysis. *Anal. Methods* **2014**, *6*, 2812–2831. [CrossRef]
172. Girin, L.; Leglaive, S.; Bie, X.; Diard, J.; Hueber, T.; Alameda-Pineda, X. Dynamical Variational Autoencoders: A Comprehensive Review. *arXiv* **2020**, arXiv:2008.12595.
173. Bank, D.; Koenigstein, N.; Giryes, R. Autoencoders. *arXiv* **2020**, arXiv:2003.05991.
174. Tschannen, M.; Bachem, O.; Lucic, M. Recent Advances in Autoencoder-Based Representation Learning. *arXiv* **2018**, arXiv:1812.05069.
175. Zhang, G.; Liu, Y.; Jin, X. A Survey of Autoencoder-Based Recommender Systems. *Front. Comput. Sci.* **2020**, *14*, 430–450. [CrossRef]
176. Verleysen, M.; François, D. The Curse of Dimensionality in Data Mining and Time Series Prediction. In Proceedings of the International Work-Conference on Artificial Neural Networks, Warsaw, Poland, 11–15 September 2005; Springer: Berlin, Germany, 2005; pp. 758–770.
177. Köppen, M. The Curse of Dimensionality. In Proceedings of the 5th Online World Conference on Soft Computing in Industrial Applications (WSC5), Virtual, 4–18 September 2000; Volume 1, pp. 4–8.
178. Poggio, T.; Mhaskar, H.; Rosasco, L.; Miranda, B.; Liao, Q. Why and When Can Deep-but Not Shallow-Networks Avoid the Curse of Dimensionality: A Review. *Int. J. Automat. Comput.* **2017**, *14*, 503–519. [CrossRef]
179. Kuo, F.Y.; Sloan, I.H. Lifting the Curse of Dimensionality. *Not. AMS* **2005**, *52*, 1320–1328.
180. Friedman, J.H. On Bias, Variance, 0/1—Loss, and the Curse-of-Dimensionality. *Data Min. Knowl. Discov.* **1997**, *1*, 55–77. [CrossRef]
181. Dohm, M.; Wang, R.; Dalton, B.; Scharenbroich, L.; Hare, M.; Castaño, R.; Baker, R. Are the Rock Compositions of the Ancient Mountain Range of Mars, Thaumasia Highlands, Distinct from Tharsis Lavas? Machine Learning Evaluation of TES Data and Implications on Early Evolution of Mars. In Proceedings of the NASA Science Technology Conference, Adelphi, MD, USA, 19–20 June 2007; pp. 1–6.
182. Dundar, M.; Ehlmann, B.L.; Leask, E. Rare Phase Detections in CRISM Data at Pixel-Scale by Machine Learning Generate New Discoveries about Geology at Mars Rover Landing Sites: Jezero and NE Syrtis. In Proceedings of the 50th Lunar and Planetary Science Conference 2019, The Woodlands, TX, USA, 18–22 March 2019.
183. Dundar, M.; Ehlmann, B.L.; Leask, E.K. Machine-Learning-Driven New Geologic Discoveries at Mars Rover Landing Sites: Jezero and NE Syrtis. *arXiv* **2019**, arXiv:1909.02387.
184. Ramachandra, V. Deep Clustering for Mars Rover Image Datasets. 2019. Available online: https://arxiv.org/abs/1911.06623 (accessed on 8 June 2022).
185. Bell, J.F.; Malin, M.C.; Caplinger, M.A.; Ravine, M.A.; Godber, A.S.; Jungers, M.C.; Rice, M.S.; Anderson, R.B. Mastcam Multispectral Imaging on the Mars Science Laboratory Rover: Wavelength Coverage and Imaging Strategies at the Gale Crater Field Site. In Proceedings of the Lunar and Planetary Science Conference, The Woodlands, TX, USA, 19–23 March 2012; p. 2541.
186. Bell, J.F., III; Godber, A.; McNair, S.; Caplinger, M.A.; Maki, J.N.; Lemmon, M.T.; van Beek, J.; Malin, M.C.; Wellington, D.; Kinch, K.M. The Mars Science Laboratory Curiosity Rover Mastcam Instruments: Preflight and In-flight Calibration, Validation, and Data Archiving. *Earth Space Sci.* **2017**, *4*, 396–452. [CrossRef]
187. Malin, M.C.; Caplinger, M.A.; Edgett, K.S.; Ghaemi, F.T.; Ravine, M.A.; Schaffner, J.A.; Baker, J.M.; Bardis, J.D.; DiBiase, D.R.; Maki, J.N. The Mars Science Laboratory (MSL) Mast-Mounted Cameras (Mastcams) Flight Instruments. In Proceedings of the 41st Annual Lunar and Planetary Science Conference, Woodlands, TX, USA, 1–5 March 2010; p. 1123.
188. Putri, A.R.D.; Sidiropoulos, P.; Muller, J.P. Anomaly Detection Performance Comparison on Anomaly-Detection Based Change Detection on Martian Image Pairs. *Int. Arch. Photogramm. Remote Sens. Spat. Inf. Sci. ISPRS Arch.* **2019**, *42*, 1437–1441. [CrossRef]
189. Castano, R.; Wagstaff, K.L.; Chien, S.; Stough, T.M.; Tang, B. On-Board Analysis of Uncalibrated Data for a Spacecraft at Mars. In Proceedings of the 13th ACM SIGKDD International Conference on Knowledge Discovery and Data Mining, San Jose, CA, USA, 12–15 August 2007; pp. 922–930. [CrossRef]
190. Sivashanmugam, M. Detecting Anomalies in Marsian Satellite Images through Object Detection. Available online: https://omdena.com/blog/mars-object-detection/?doing_wp_cron=1646425605.3414530754089355468750 (accessed on 8 June 2022).
191. Rajaneesh, A.; Vishnu, C.L.; Oommen, T.; Rajesh, V.J.; Sajinkumar, K.S. Machine Learning as a Tool to Classify Extra-Terrestrial Landslides: A Dossier from Valles Marineris, Mars. *Icarus* **2022**, *376*, 114886. [CrossRef]
192. Scuderi, L.A.; Nagle-McNaughton, T. Automated Neural Network Identification of Cirques. *Phys. Geogr.* **2022**, *43*, 24–51. [CrossRef]
193. Alimo, R.; Sam, D.; Lakhmiri, D.; Kahovec, B.; Divsalar, D. Automated Data Accountability for Missions in Mars Rover Data. In Proceedings of the 2021 IEEE Aerospace Conference, Big Sky, MT, USA, 6–13 March 2021. [CrossRef]
194. van Engelen, J.E.; Hoos, H.H. A Survey on Semi-Supervised Learning. *Mach. Learn.* **2020**, *109*, 373–440. [CrossRef]

195. Zhou, X.; Belkin, M. Semi-Supervised Learning. In *Academic Press Library in Signal Processing*; Elsevier: Amsterdam, The Netherlands, 2014; Volume 1, pp. 1239–1269. ISBN 2351-9819.
196. Zhu, X.; Goldberg, A.B. Introduction to Semi-Supervised Learning. *Synth. Lect. Artif. Intell. Mach. Learn.* **2009**, *3*, 1–130.
197. Li, Y.-F.; Zhou, Z.-H. Towards Making Unlabeled Data Never Hurt. *IEEE Trans. Pattern Anal. Mach. Intell.* **2014**, *37*, 175–188.
198. Singh, A.; Nowak, R.; Zhu, J. Unlabeled Data: Now It Helps, Now It Doesn't. In Proceedings of the Twenty-Second Annual Conference on Neural Information Processing Systems, Vancouver, BC, Canada, 8–11 December 2008.
199. Wang, W.; Lin, L.; Fan, Z.; Liu, J. Semi-Supervised Learning for Mars Imagery Classification. In Proceedings of the 2021 IEEE International Conference on Image Processing, Anchorage, AK, USA, 19–22 September 2021; pp. 499–503. [CrossRef]
200. Goh, E.; Chen, J.; Wilson, B. Mars Terrain Segmentation with Less Labels. *arXiv* **2022**, arXiv:2202.00791.
201. Khosla, P.; Teterwak, P.; Wang, C.; Sarna, A.; Tian, Y.; Isola, P.; Maschinot, A.; Liu, C.; Krishnan, D. Supervised Contrastive Learning. *Adv. Neural Inf. Process. Syst.* **2020**, *33*, 18661–18673.
202. Chen, T.; Kornblith, S.; Norouzi, M.; Hinton, G. A Simple Framework for Contrastive Learning of Visual Representations. In Proceedings of the International Conference on Machine Learning, Virtual, 13–18 July 2020; pp. 1597–1607.
203. Lu, S.; Wagstaff, K.L. MSL Curiosity Rover Images with Science and Engineering Classes. 2020. Available online: https://zenodo.org/record/4033453#.YqlotexBxPY (accessed on 8 June 2022). [CrossRef]
204. Devlin, J.; Chang, M.-W.; Lee, K.; Toutanova, K. Bert: Pre-Training of Deep Bidirectional Transformers for Language Understanding. *arXiv* **2018**, arXiv:1810.04805.
205. Dale, R. GPT-3: What's It Good for? *Nat. Lang. Eng.* **2021**, *27*, 113–118. [CrossRef]
206. Brown, T.; Mann, B.; Ryder, N.; Subbiah, M.; Kaplan, J.D.; Dhariwal, P.; Neelakantan, A.; Shyam, P.; Sastry, G.; Askell, A. Language Models Are Few-Shot Learners. *Adv. Neural Inf. Process. Syst.* **2020**, *33*, 1877–1901.
207. Floridi, L.; Chiriatti, M. GPT-3: Its Nature, Scope, Limits, and Consequences. *Minds Mach.* **2020**, *30*, 681–694. [CrossRef]
208. Gui, J.; Sun, Z.; Wen, Y.; Tao, D.; Ye, J. A Review on Generative Adversarial Networks: Algorithms, Theory, and Applications. *IEEE Trans. Knowl. Data Eng.* **2021**. *Preprints* . [CrossRef]
209. Gonog, L.; Zhou, Y. A Review: Generative Adversarial Networks. In Proceedings of the 14th IEEE Conference on Industrial Electronics and Applications (ICIEA), Xi'an, China, 9–21 June 2019; Institute of Electrical and Electronics Engineers (IEEE): Piscataway, NJ, USA, 2019; pp. 505–510.
210. Alqahtani, H.; Kavakli-Thorne, M.; Kumar, G. Applications of Generative Adversarial Networks (Gans): An Updated Review. *Arch. Comput. Methods Eng.* **2021**, *28*, 525–552. [CrossRef]
211. Karras, T.; Laine, S.; Aittala, M.; Hellsten, J.; Lehtinen, J.; Aila, T. Analyzing and Improving the Image Quality of Stylegan. In Proceedings of the IEEE/CVF Conference on Computer Vision and Pattern Recognition, Seattle, WA, USA, 13–19 June 2020; pp. 8110–8119.
212. Karras, T.; Laine, S.; Aila, T. A Style-Based Generator Architecture for Generative Adversarial Networks. *IEEE Trans. Pattern Anal. Mach. Intell.* **2021**, *43*, 4217–4228. [CrossRef] [PubMed]
213. Hussein, S.A.; Tirer, T.; Giryes, R. Image-Adaptive GAN Based Reconstruction. In Proceedings of the AAAI Conference on Artificial Intelligence, New York, NY, USA, 7–12 February 2020; Volume 34, pp. 3121–3129.
214. Shoshan, A.; Bhonker, N.; Kviatkovsky, I.; Medioni, G. Gan-Control: Explicitly Controllable Gans. In Proceedings of the IEEE/CVF International Conference on Computer Vision, Montreal, Canada, 11–17 October 2021; pp. 14083–14093.
215. Karras, T.; Aila, T. Training Generative Adversarial Networks with Limited Data Paper. In Proceedings of the NeurIPS 2020, Virtual, 6–12 December 2020.
216. Zhu, M.; Pan, P.; Chen, W.; Yang, Y. Dm-Gan: Dynamic Memory Generative Adversarial Networks for Text-to-Image Synthesis. In Proceedings of the IEEE/CVF Conference on Computer Vision and Pattern Recognition, Long Beach, CA, USA, 15–20 June 2019; pp. 5802–5810.
217. Tao, M.; Tang, H.; Wu, S.; Sebe, N.; Jing, X.-Y.; Wu, F.; Bao, B. Df-Gan: Deep Fusion Generative Adversarial Networks for Text-to-Image Synthesis. *arXiv* **2020**, arXiv:2008.05865.
218. Wang, H.; Lin, G.; Hoi, S.C.H.; Miao, C. Cycle-Consistent Inverse Gan for Text-to-Image Synthesis. In Proceedings of the 29th ACM International Conference on Multimedia, Chengdu, China, 21–25 October 2021; pp. 630–638.
219. Cai, Y.; Wang, X.; Yu, Z.; Li, F.; Xu, P.; Li, Y.; Li, L. Dualattn-GAN: Text to Image Synthesis with Dual Attentional Generative Adversarial Network. *IEEE Access* **2019**, *7*, 183706–183716. [CrossRef]
220. Ruan, S.; Zhang, Y.; Zhang, K.; Fan, Y.; Tang, F.; Liu, Q.; Chen, E. Dae-Gan: Dynamic Aspect-Aware Gan for Text-to-Image Synthesis. In Proceedings of the IEEE/CVF International Conference on Computer Vision, Montreal, Canada, 11–17 October 2021; pp. 13960–13969.
221. Chu, M.; Xie, Y.; Leal-Taixé, L.; Thuerey, N. Temporally Coherent Gans for Video Super-Resolution (Tecogan). *arXiv* **2018**, arXiv:1811.09393.
222. Demiray, B.Z.; Sit, M.; Demir, I. D-SRGAN: DEM Super-Resolution with Generative Adversarial Networks. *SN Comput. Sci.* **2021**, *2*, 48. [CrossRef]
223. Park, S.-J.; Son, H.; Cho, S.; Hong, K.-S.; Lee, S. Srfeat: Single Image Super-Resolution with Feature Discrimination. In Proceedings of the European conference on computer vision (ECCV), Munich, Germany, 8–14 September 2018; pp. 439–455.
224. Mahapatra, D.; Bozorgtabar, B.; Garnavi, R. Image Super-Resolution Using Progressive Generative Adversarial Networks for Medical Image Analysis. *Comput. Med. Imaging Graph.* **2019**, *71*, 30–39. [CrossRef]

225. Ledig, C.; Theis, L.; Huszár, F.; Caballero, J.; Cunningham, A.; Acosta, A.; Aitken, A.; Tejani, A.; Totz, J.; Wang, Z. Photo-Realistic Single Image Super-Resolution Using a Generative Adversarial Network. In Proceedings of the IEEE Conference on Computer Vision and Pattern Recognition, Honolulu, HI, USA, 21–26 June 2017; pp. 4681–4690.
226. Bulat, A.; Tzimiropoulos, G. Super-Fan: Integrated Facial Landmark Localization and Super-Resolution of Real-World Low Resolution Faces in Arbitrary Poses with Gans. In Proceedings of the IEEE Conference on Computer Vision and Pattern Recognition, Salt Lake City, UT, USA, 18–22 June 2018; pp. 109–117.
227. Yang, W.; Zhang, X.; Tian, Y.; Wang, W.; Xue, J.-H.; Liao, Q. Deep Learning for Single Image Super-Resolution: A Brief Review. *IEEE Trans. Multimed.* **2019**, *21*, 3106–3121. [CrossRef]
228. Gupta, R.; Sharma, A.; Kumar, A. Super-Resolution Using GANs for Medical Imaging. *Procedia Comput. Sci.* **2020**, *173*, 28–35. [CrossRef]
229. Ma, J.; Yu, W.; Chen, C.; Liang, P.; Guo, X.; Jiang, J. Pan-GAN: An Unsupervised Pan-Sharpening Method for Remote Sensing Image Fusion. *Inf. Fusion* **2020**, *62*, 110–120. [CrossRef]
230. Diao, W.; Zhang, F.; Sun, J.; Xing, Y.; Zhang, K.; Bruzzone, L. ZeRGAN: Zero-Reference GAN for Fusion of Multispectral and Panchromatic Images. *IEEE Trans. Neural Netw. Learn. Syst.* **2022**, 1–15. [CrossRef]
231. Tao, Y.; Conway, S.J.; Mulle, J.P.; Putri, A.R.D.; Thomas, N.; Cremonese, G. Single Image Super-Resolution Restoration of TGO Cassis Colour Images: Demonstration with Perseverance Rover Landing Site and Mars Science Targets. *Remote Sens.* **2021**, *13*, 1777. [CrossRef]
232. Wang, C.; Zhang, Y.; Zhang, Y.; Tian, R.; Ding, M. Mars Image Super-Resolution Based on Generative Adversarial Network. *IEEE Access* **2021**, *9*, 108889–108898. [CrossRef]
233. Tao, Y.; Muller, J.P.; Xiong, S.; Conway, S.J. MADnet 2.0: Pixel-Scale Topography Retrieval from Single-View Orbital Imagery of Mars Using Deep Learning. *Remote Sens.* **2021**, *13*, 4220. [CrossRef]
234. Tao, Y.; Muller, J.P.; Conway, S.J.; Xiong, S. Large Area High-Resolution 3d Mapping of Oxia Planum: The Landing Site for the Exomars Rosalind Franklin Rover. *Remote Sens.* **2021**, *13*, 3270. [CrossRef]
235. Tao, Y.; Douté, S.; Muller, J.P.; Conway, S.J.; Thomas, N.; Cremonese, G. Ultra-High-Resolution 1 m/Pixel CaSSIS DTM Using Super-Resolution Restoration and Shape-from-Shading: Demonstration over Oxia Planum on Mars. *Remote Sens.* **2021**, *13*, 2185. [CrossRef]
236. Brooks, C.A.; Iagnemma, K.D. Self-Supervised Classification for Planetary Rover Terrain Sensing. In Proceedings of the 2007 IEEE Aerospace Conference, Big Sky, MT, USA, 3–10 March 2007; pp. 1–9. [CrossRef]
237. Brierley, G.; Fryirs, K.; Reid, H.; Williams, R. The Dark Art of Interpretation in Geomorphology. *Geomorphology* **2021**, *390*, 107870. [CrossRef]
238. Haines-Young, R.H.; Petch, J.R. *Multiple Working Hypotheses: Equifinality and the Study of Landforms*; University of Salford, Department of Geography: Salford, UK, 1983; pp. 458–466.
239. Schumm, S.A.; Schumm, S.A. *To Interpret the Earth: Ten Ways to Be Wrong*; Cambridge University Press: Cambridge, UK, 1998; ISBN 0521646022.
240. Balaji, V. Climbing down Charney's Ladder: Machine Learning and the Post-Dennard Era of Computational Climate Science. *Philos. Trans. R. Soc. A* **2021**, *379*, 20200085. [CrossRef] [PubMed]
241. Church, M. The Trajectory of Geomorphology. *Prog. Phys. Geogr. Earth Environ.* **2010**, *34*, 265–286. [CrossRef]
242. Banham, S.G.; Gupta, S.; Rubin, D.M.; Edgett, K.S.; Barnes, R.; van Beek, J.; Watkins, J.A.; Edgar, L.A.; Fedo, C.M.; Williams, R.M. A Rock Record of Complex Aeolian Bedforms in a Hesperian Desert Landscape: The Stimson Formation as Exposed in the Murray Buttes, Gale Crater, Mars. *J. Geophys. Res. Planets* **2021**, *126*, e2020JE006554. [CrossRef]
243. Horvath, D.G.; Andrews-Hanna, J.C. The Hydrology and Climate of Mars during the Sedimentary Infilling of Gale Crater. *Earth Planet. Sci. Lett.* **2021**, *568*, 117032. [CrossRef]
244. Rapin, W.; Dromart, G.; Rubin, D.; Le Deit, L.; Mangold, N.; Edgar, L.A.; Gasnault, O.; Herkenhoff, K.; le Mouélic, S.; Anderson, R.B. Alternating Wet and Dry Depositional Environments Recorded in the Stratigraphy of Mount Sharp at Gale Crater, Mars. *Geology* **2021**, *49*, 842–846. [CrossRef]
245. Liu, J.; Michalski, J.R.; Zhou, M.-F. Intense Subaerial Weathering of Eolian Sediments in Gale Crater, Mars. *Sci. Adv.* **2021**, *7*, eabh2687. [CrossRef]
246. Cummings, T.G.; Worley, C.G. *Organization Development and Change*; Cengage Learning: Boston, MA, USA, 2014; ISBN 1305143035.
247. Williams, J.M.; Scuderi, L.A.; Newsom, H.E. Numerical Analysis of Putative Rock Glaciers on Mount Sharp, Gale Crater, Mars. *Remote Sens.* **2022**, *14*, 1887. [CrossRef]
248. Church, M. *Space, Time and the Mountain–How Do We Order What We See*; Wiley: New York, NY, USA, 1996.
249. Day, M.; Zimbelman, J.R. Ripples, Megaripples, and TARs, Oh, My! Recommendations Regarding Mars Aeolian Bedform Terminology. *Icarus* **2021**, *369*, 114647. [CrossRef]
250. Nagle-McNaughton, T.P.; Scuderi, L.A. Multistage Evolution in Transverse Aeolian Ridges. *Remote Sens.* **2021**, *13*, 1329. [CrossRef]
251. Geissler, P.E.; Wilgus, J.T. The Morphology of Transverse Aeolian Ridges on Mars. *Aeolian Res.* **2017**, *26*, 63–71. [CrossRef]
252. Nagle-McNaughton, T.P.; Scuderi, L.A. A Geomorphological Case for Multistage Evolution of Transverse Aeolian Ridges. *Planet. Space Sci.* **2021**, *200*, 105192. [CrossRef]
253. Geissler, P.E. The Birth and Death of Transverse Aeolian Ridges on Mars. *J. Geophys. Res. Planets* **2014**, 2583–2599. [CrossRef]

254. Zimbelman, J.R.; Williams, S.H. An Evaluation of Formation Processes for Transverse Aeolian Ridges on Mars. In Proceedings of the Seventh International Conference on Mars, Pasadena, CA, USA, 9–13 July 2007; LPI Contribution No. 1353. p. 3047.
255. Hugenholtz, C.H.; Barchyn, T.E. A Terrestrial Analog for Transverse Aeolian Ridges (TARs): Environment, Morphometry, and Recent Dynamics. *Icarus* **2017**, *289*, 239–253. [CrossRef]
256. Wilson, S.A.; Zimbelman, J.R. Latitude-Dependent Nature and Physical Characteristics of Transverse Aeolian Ridges on Mars. *J. Geophys. Res. E Planets* **2004**, *109*, 1–12. [CrossRef]
257. Foroutan, M.; Zimbelman, J.R. Mega-Ripples in Iran: A New Analog for Transverse Aeolian Ridges on Mars. *Icarus* **2016**, *274*, 99–105. [CrossRef]
258. Hugenholtz, C.H.; Barchyn, T.E.; Boulding, A. Morphology of Transverse Aeolian Ridges (TARs) on Mars from a Large Sample: Further Evidence of a Megaripple Origin? *Icarus* **2017**, *286*, 193–201. [CrossRef]
259. Zimbelman, J.R.; Scheidt, S.P. Precision Topography of a Reversing Sand Dune at Bruneau Dunes, Idaho, as an Analog for Transverse Aeolian Ridges on Mars. *Icarus* **2014**, *230*, 29–37. [CrossRef]
260. Kereszturi, A.; Aszalos, J.M.; Zs, H.; Igneczi, Á.; Zs, K.; Cs, K.; Sz, L.O.; Szalai, Z.; Zs, N.; Pal, B.; et al. Wind-Snow Interactions at the Ojos Del Salado Region as a Potential Mars Analogue Site in the Altiplano—Atacama Desert Region. *Icarus* **2022**, *378*, 114941. [CrossRef]
261. Held, I.M. The Gap between Simulation and Understanding in Climate Modeling. *Bull. Am. Meteorol. Soc.* **2005**, *86*, 1609–1614. [CrossRef]
262. Li, Y.; Zhao, Z. AutoCirque: An Automated Method to Delineate Glacial Cirque Outlines from Digital Elevation Models. *Geomorphology* **2022**, *398*, 108059. [CrossRef]
263. Fernández, M.M.; Yue, Y.; Weber, R. Telemetry Anomaly Detection System Using Machine Learning to Streamline Mission Operations. In Proceedings of the 2017 6th International Conference on Space Mission Challenges for Information Technology (SMC-IT), Virtual, 26–30 July 2017; Institute of Electrical and Electronics Engineers (IEEE): Piscataway, NJ, USA, 2017; pp. 70–75.
264. Lakhmiri, D.; Alimo, R.; le Digabel, S. Anomaly Detection for Data Accountability of Mars Telemetry Data. *Expert Syst. Appl.* **2022**, *189*, 116060. [CrossRef]
265. Kostovska, A.; Petković, M.; Stepišnik, T.; Lucas, L.; Finn, T.; Martínez-Heras, J.; Panov, P.; Džeroski, S.; Donati, A.; Simidjievski, N. GalaxAI: Machine Learning Toolbox for Interpretable Analysis of Spacecraft Telemetry Data. *arXiv* **2021**, arXiv:2108.01407.
266. Gaudet, B.; Furfaro, R. Adaptive Pinpoint and Fuel Efficient Mars Landing Using Reinforcement Learning. *IEEE/CAA J. Autom. Sin.* **2014**, *1*, 397–411.
267. Petković, M.; Boumghar, R.; Breskvar, M.; Džeroski, S.; Kocev, D.; Levatić, J.; Lucas, L.; Osojnik, A.; Ženko, B.; Simidjievski, N. Machine Learning for Predicting Thermal Power Consumption of the Mars Express Spacecraft. *IEEE Aerosp. Electron. Syst. Mag.* **2019**, *34*, 46–60. [CrossRef]
268. Furfaro, R.; Scorsoglio, A.; Linares, R.; Massari, M. Adaptive Generalized ZEM-ZEV Feedback Guidance for Planetary Landing via a Deep Reinforcement Learning Approach. *Acta Astronaut.* **2020**, *171*, 156–171. [CrossRef]
269. Izzo, D.; Sprague, C.I.; Tailor, D.V. Machine Learning and Evolutionary Techniques in Interplanetary Trajectory Design. In *Modeling and Optimization in Space Engineering*; Springer: New York, NY, USA, 2019; pp. 191–210.
270. Ampatzis, C.; Izzo, D. Machine Learning Techniques for Approximation of Objective Functions in Trajectory Optimisation. In Proceedings of the IJCAI-09 Workshop on Artificial Intelligence in Space, Pasadena, CA, USA, 11–13 July 2009; pp. 1–6.
271. Furfaro, R.; Simo, J.; Gaudet, B.; Wibben, D. Neural-Based Trajectory Shaping Approach for Terminal Planetary Pinpoint Guidance. In Proceedings of the AAS/AIAA Astrodynamics Specialist Conference 2013, Hilton Head, South Carolina, 11–15 August 2013.
272. Boumghar, R.; Lucas, L.; Donati, A. Machine Learning in Operations for the Mars Express Orbiter. In Proceedings of the 2018 SpaceOps Conference 2018, Marseille, France, 28 May–1 June 2018; p. 2551.
273. Golombek, M.P.; Huertas, A.; Marlow, J.; McGrane, B.; Klein, C.; Martinez, M.; Arvidson, R.E.; Heet, T.; Barry, L.; Seelos, K.; et al. Size-Frequency Distributions of Rocks on the Northern Plains of Mars with Special Reference to Phoenix Landing Surfaces. *J. Geophys. Res. E Planets* **2009**, *114*, 1–32. [CrossRef]
274. Golombek, M.P.; Haldemann, A.F.C.; Forsberg-Taylor, N.K.; DiMaggio, E.N.; Schroeder, R.D.; Jakosky, B.M.; Mello, M.T.; Matijevic, J.R. Rock Size-Frequency Distributions on Mars and Implications for Mars Exploration Rover Landing Safety and Operations. *J. Geophys. Res. E Planets* **2003**, *108*. [CrossRef]
275. Arvidson, R.; Adams, D.; Bonfiglio, G.; Christensen, P.; Cull, S.; Golombek, M.; Guinn, J.; Guinness, E.; Heet, T.; Kirk, R. Mars Exploration Program 2007 Phoenix Landing Site Selection and Characteristics. *J. Geophys. Res. Planets* **2008**, *113*. [CrossRef]
276. Grant, J.A.; Golombek, M.P.; Wilson, S.A.; Farley, K.A.; Williford, K.H.; Chen, A. The Science Process for Selecting the Landing Site for the 2020 Mars Rover. *Planet. Space Sci.* **2018**, *164*, 106–126. [CrossRef]
277. Grant, J.A.; Wilson, S.A.; Ruff, S.W.; Golombek, M.P.; Koestler, D.L. Distribution of Rocks on the Gusev Plains and on Husband Hill, Mars. *Geophys. Res. Lett.* **2006**, *33*. [CrossRef]
278. Craddock, R.A.; Golombek, M.P.; Howard, A.D. Analyses of Rock Size-Frequency Distributions and Morphometry of Modified Hawaiian Lava Flows: Implications for Future Martian Landing Sites. In Proceedings of the 31st Annual Lunar and Planetary Science Conference, Houston, TX, USA, 13–17 March 2000.
279. Golombek, M.; Huertas, A.; Kipp, D.; Calef, F. Detection and Characterization of Rocks and Rock Size-Frequency Distributions at the Final Four Mars Science Laboratory Landing Sites. *Mars* **2012**, *7*, 1–22. [CrossRef]

280. Huertas, A.; Cheng, Y.; Madison, R. Passive Imaging Based Multi-Cue Hazard Detection for Spacecraft Safe Landing. In Proceedings of the 2006 IEEE Aerospace Conference, Big Sky, Montana, USA, 4–11 March 2006; Institute of Electrical and Electronics Engineers (IEEE): Piscataway, NJ, USA, 2006; p. 14.
281. Ivanov, M.A.; Slyuta, E.N.; Grishakina, E.A.; Dmitrovskii, A.A. Geomorphological Analysis of ExoMars Candidate Landing Site Oxia Planum. *Sol. Syst. Res.* **2020**, *54*, 1–14. [CrossRef]
282. Mastropietro, M.; Pajola, M.; Cremonese, G.; Munaretto, G.; Lucchetti, A. Boulder Analysis on the Oxia Planum ExoMars 2022 Rover Landing Site: Scientific and Engineering Perspectives. *Sol. Syst. Res.* **2020**, *54*, 504–519. [CrossRef]
283. Masursky, H.; Chapman, M.G.; Davis, P.A.; Dial, A.L., Jr.; Strobell, M.E. Mars Lander/Rover/Returned Sample Sites. In Proceedings of the Lunar and Planetary Science Conference 1987, Houston, TX USA, 16–20 March 1987; Volume 18.
284. Ward, J.G.; Arvidson, R.E.; Golombek, M. The Size-Frequency and Areal Distribution of Rock Clasts at the Spirit Landing Site, Gusev Crater, Mars. *Geophys. Res. Lett.* **2005**, *32*, 1–4. [CrossRef]
285. Putzig, N.E.; Phillips, R.J.; Campbell, B.A.; Mellon, M.T.; Holt, J.W.; Brothers, T.C. SHARAD Soundings and Surface Roughness at Past, Present, and Proposed Landing Sites on Mars: Reflections at Phoenix May Be Attributable to Deep Ground Ice. *J. Geophys. Res. Planets* **2014**, *119*, 1936–1949. [CrossRef]
286. Matthies, L.; Huertas, A.; Cheng, Y.; Johnson, A. Landing Hazard Detection with Stereo Vision and Shadow Analysis. In Proceedings of the 2007 AIAA InfoTech at Aerospace Conference, Rohnert Park, CA, USA, 7–10 May 2007; American Institute of Aeronautics and Astronautics: Reston, VA, USA; Volume 2, pp. 1284–1293, ISBN 1563478935.
287. Ishraque, F.; Levy, J.S. Detection of Boulder Banding on Martian Lobate Debris Aprons Using Regional Convolutional Neural Network Analysis of HiRISE Image Data. In Proceedings of the 53rd Lunar and Planetary Science Conference, The Woodlands, TX, USA, 7–11 March, 2022. LPI Contribution No. 2678, 2022, id.2875.
288. Moeller, R.C.; Jandura, L.; Rosette, K.; Robinson, M.; Samuels, J.; Silverman, M.; Brown, K.; Duffy, E.; Yazzie, A.; Jens, E. The Sampling and Caching Subsystem (SCS) for the Scientific Exploration of Jezero Crater by the Mars 2020 Perseverance Rover. *Space Sci. Rev.* **2021**, *217*, 5. [CrossRef]
289. Mangold, N.; Gupta, S.; Gasnault, O.; Dromart, G.; Tarnas, J.D.; Sholes, S.F.; Horgan, B.; Quantin-Nataf, C.; Brown, A.J.; le Mouélic, S. Perseverance Rover Reveals an Ancient Delta-Lake System and Flood Deposits at Jezero Crater, Mars. *Science* **2021**, *374*, 711–717. [CrossRef]
290. Nagle-McNaughton, T.P.; Williams, J.M.; Gallegos, Z.E.; Wilkie, H.A.; Martinez, D.C.; Scuderi, L.A. Geographic Information System Based Detection and Quantification of Boulders Using HiRISE Imagery: A Case Study in Jezero Crater. *J. Appl. Remote Sens.* **2020**, *14*, 1. [CrossRef]
291. Golombek, M.; Kass, D.; Williams, N.; Warner, N.; Daubar, I.; Piqueux, S.; Charalambous, C.; Pike, W.T. Assessment of InSight Landing Site Predictions. *J. Geophys. Res. Planets* **2020**, *125*, e2020JE006502. [CrossRef]
292. Quantin-Nataf, C.; Carter, J.; Mandon, L.; Thollot, P.; Balme, M.; Volat, M.; Pan, L.; Loizeau, D.; Millot, C.; Breton, S. Oxia Planum: The Landing Site for the ExoMars "Rosalind Franklin" Rover Mission: Geological Context and Prelanding Interpretation. *Astrobiology* **2021**, *21*, 345–366. [CrossRef] [PubMed]
293. Kereszturi, A. Landing Site Rationality Scaling for Subsurface Sampling on Mars—Case Study for ExoMars Rover-like Missions. *Planet. Space Sci.* **2012**, *72*, 78–90. [CrossRef]
294. Fairén, A.G.; Dohm, J.M.; Baker, V.R.; de Pablo, M.A.; Ruiz, J.; Ferris, J.C.; Anderson, R.C. Episodic Flood Inundations of the Northern Plains of Mars. *Icarus* **2003**, *165*, 53–67. [CrossRef]
295. Di Achille, G.; Hynek, B.M. Ancient Ocean on Mars Supported by Global Distribution of Deltas and Valleys. *Nat. Geosci.* **2010**, *3*, 459–463. [CrossRef]
296. de Toffoli, B.; Plesa, A.; Hauber, E.; Breuer, D. Delta Deposits on Mars: A Global Perspective. *Geophys. Res. Lett.* **2021**, *48*, e2021GL094271. [CrossRef]
297. Di Achille, G.; Ori, G.G.; Reiss, D. Evidence for Late Hesperian Lacustrine Activity in Shalbatana Vallis, Mars. *J. Geophys. Res. Planets* **2007**, *112*. [CrossRef]
298. Erkeling, G.; Reiss, D.; Hiesinger, H.; Poulet, F.; Carter, J.; Ivanov, M.A.; Hauber, E.; Jaumann, R. Valleys, Paleolakes and Possible Shorelines at the Libya Montes/Isidis Boundary: Implications for the Hydrologic Evolution of Mars. *Icarus* **2012**, *219*, 393–413. [CrossRef]
299. Balme, M.; Berman, D.C.; Bourke, M.C.; Zimbelman, J.R. Transverse Aeolian Ridges (TARs) on Mars. *Geomorphology* **2008**, *101*, 703–720. [CrossRef]
300. Berman, D.C.; Balme, M.R.; Michalski, J.R.; Clark, S.C.; Joseph, E.C.S. High-Resolution Investigations of Transverse Aeolian Ridges on Mars. *Icarus* **2018**, *312*, 247–266. [CrossRef]
301. Berman, D.C.; Balme, M.R.; Rafkin, S.C.R.; Zimbelman, J.R. Transverse Aeolian Ridges (TARs) on Mars II: Distributions, Orientations, and Ages. *Icarus* **2011**, *213*, 116–130. [CrossRef]
302. Sullivan, R.; Bridges, N.; Herkenhoff, K.; Hamilton, V.; Rubin, D. Transverse Aeolian Ridges (TARs) as Megaripples: Rover Encounters at Meridiani Planum, Gusev, and Gale. In Proceedings of the Eighth International Conference on Mars 2014, Pasadena, CA, USA, 14–18 July 2014; Volume 1791, p. 1424.
303. Scuderi, L.; Nagle-McNaughton, T.; Williams, J. Trace Evidence from Mars' Past: Fingerprinting Transverse Aeolian Ridges. *Remote Sens.* **2019**, *11*, 1060. [CrossRef]

304. Nagle-McNaughton, T.P.; Scuderi, L.A. Networked Configurations as an Emergent Property of Transverse Aeolian Ridges on Mars. *Commun. Earth Environ.* **2021**, *2*, 217. [CrossRef]
305. Silvestro, S.; Chojnacki, M.; Vaz, D.A.; Cardinale, M.; Yizhaq, H.; Esposito, F. Megaripple Migration on Mars. *J. Geophys. Res. Planets* **2020**, *125*, e2020JE006446. [CrossRef] [PubMed]
306. Sullivan, R.; Kok, J.F.; Katra, I.; Yizhaq, H. A Broad Continuum of Aeolian Impact Ripple Morphologies on Mars Is Enabled by Low Wind Dynamic Pressures. *J. Geophys. Res. Planets* **2020**, *125*, e2020JE006485. [CrossRef]
307. Andreotti, B.; Claudin, P.; Iversen, J.J.; Merrison, J.P.; Rasmussen, K.R. A Lower-than-Expected Saltation Threshold at Martian Pressure and Below. *Proc. Natl. Acad. Sci. USA* **2021**, *118*, e2012386118. [CrossRef]
308. Hugenholtz, C.H.; Barchyn, T.E.; Favaro, E.A. Formation of Periodic Bedrock Ridges on Earth. *Aeolian Res.* **2015**, *18*, 135–144. [CrossRef]
309. Silvestro, S.; Pacifici, A.; Salese, F.; Vaz, D.A.; Neesemann, A.; Tirsch, D.; Popa, C.I.; Pajola, M.; Franzese, G.; Mongelluzzo, G. Periodic Bedrock Ridges at the ExoMars 2022 Landing Site: Evidence for a Changing Wind Regime. *Geophys. Res. Lett.* **2021**, *48*, e2020GL091651. [CrossRef]
310. Montgomery, D.R.; Bandfield, J.L.; Becker, S.K. Periodic Bedrock Ridges on Mars. *J. Geophys. Res. E Planets* **2012**, *117*, 1–12. [CrossRef]
311. Stack, K.; Arvidson, R.E.; Bennett, K.A.; Bryk, A.B.; Edgett, K.S.; Fedo, C.; Fox, V.K.; Fraeman, A.; House, C.H.; Rabinovitch, J. In-Situ Investigation of Periodic Bedrock Ridges in the Glen Torridon Area with the MSL Curiosity Rover, Gale Crater, Mars. In Proceedings of the AGU Fall Meeting Abstracts 2019, San Francisco, CA, USA, 9–13 December 2019; Volume 2019, p. P33B-02.
312. Horváth, A.; Kereszturi, Á.; Bérczi, S.; Sik, A.; Pócs, T.; Gánti, T.; Szathmáry, E. Analysis of Dark Albedo Features on a Southern Polar Dune Field of Mars. *Astrobiology* **2009**, *9*, 90–103. [CrossRef]
313. Kereszturi, A.; Vincendon, M.; Schmidt, F. Water Ice in the Dark Dune Spots of Richardson Crater on Mars. *Planet. Space Sci.* **2011**, *59*, 26–42. [CrossRef]
314. Gánti, T.; Horváth, A.; Bérczi, S.; Gesztesi, A.; Szathmáry, E. Dark Dune Spots: Possible Biomarkers on Mars? *Orig. Life Evol. Biosph.* **2003**, *33*, 515–557. [CrossRef] [PubMed]
315. Pain, C.F.; Oilier, C.D. Inversion of Relief—A Component of Landscape Evolution. *Geomorphology* **1995**, *12*, 151–165. [CrossRef]
316. Pain, C.F.; Clarke, J.D.A.; Thomas, M. Inversion of Relief on Mars. *Icarus* **2007**, *190*, 478–491. [CrossRef]
317. Newsom, H.E.; Lanza, N.L.; Ollila, A.M.; Wiseman, S.M.; Roush, T.L.; Marzo, G.A.; Tornabene, L.L.; Okubo, C.H.; Osterloo, M.M.; Hamilton, V.E. Inverted Channel Deposits on the Floor of Miyamoto Crater, Mars. *Icarus* **2010**, *205*, 64–72. [CrossRef]
318. Golombek, M.P.; Bridges, N.T. Erosion Rates on Mars and Implications for Climate Change: Constraints from the Pathfinder Landing Site. *J. Geophys. Res. Planets* **2000**, *105*, 1841–1853. [CrossRef]
319. Golombek, M.P.; Grant, J.A.; Crumpler, L.S.; Greeley, R.; Arvidson, R.E.; Bell, J.F., III; Weitz, C.M.; Sullivan, R.; Christensen, P.R.; Soderblom, L.A. Erosion Rates at the Mars Exploration Rover Landing Sites and Long-term Climate Change on Mars. *J. Geophys. Res. Planets* **2006**, *111*, E12S10. [CrossRef]
320. Williams, R.M.E.; Irwin, R.P., III; Zimbelman, J.R. Evaluation of Paleohydrologic Models for Terrestrial Inverted Channels: Implications for Application to Martian Sinuous Ridges. *Geomorphology* **2009**, *107*, 300–315. [CrossRef]
321. Hoke, M.R.T.; Hynek, B.M.; Tucker, G.E. Formation Timescales of Large Martian Valley Networks. *Earth Planet. Sci. Lett.* **2011**, *312*, 1–12. [CrossRef]
322. Kite, E.S.; Mayer, D.P.; Wilson, S.A.; Davis, J.M.; Lucas, A.S.; Stucky de Quay, G. Persistence of Intense, Climate-Driven Runoff Late in Mars History. *Sci. Adv.* **2019**, *5*, eaav7710. [CrossRef]
323. Carr, M.H. The Fluvial History of Mars. *Philos. Trans. R. Soc. A Math. Phys. Eng. Sci.* **2012**, *370*, 2193–2215. [CrossRef]
324. Leask, E.K.; Ehlmann, B.L. Evidence for Deposition of Chloride on Mars from Small-volume Surface Water Events into the Late Hesperian-Early Amazonian. *AGU Adv.* **2022**, *3*, e2021AV000534. [CrossRef]
325. Nizam, N.; Divola, C.; Day, M.; Yin, A.; Moon, S. Development of Chaos Terrain as Subaqueous Slide Blocks in Galilaei Crater, Mars. *Remote Sens.* **2022**, *14*, 1998. [CrossRef]
326. King, I.; Kuentz, L.; Rapoza, M.C.; Kuang, L.; Wang, H.; Levy, J. Geomorphic Analysis of Mars Chaos Terrains Using Global CTX Mosaic, HIRISE, and MOLA-HRSC Blended DEM Global Imagery: Fracture Density and Block Thickness Suggest Basin Control of Chaotically-Cracked Units. In Proceedings of the 53rd Lunar and Planetary Science Conference, The Woodlands, TX, USA, 7–11 March 2022; Volume 2678, p. 1210.
327. Shozaki, H.; Sekine, Y.; Guttenberg, N. Classification of Martian Chaos Terrains Using Imagery Machine Learning: Implications for Ground Ice Distributions and Dynamics. In Proceedings of the AGU Fall Meeting Abstracts 2020, Virtual Conference, 1–17 December 2020; p. P042-0011.
328. Skjetne, H.L.; Singer, K.N.; Hynek, B.M.; Knight, K.I.; Schenk, P.M.; Olkin, C.B.; White, O.L.; Bertrand, T.; Runyon, K.D.; McKinnon, W.B. Morphological Comparison of Blocks in Chaos Terrains on Pluto, Europa, and Mars. *Icarus* **2021**, *356*, 113866. [CrossRef]
329. Trumbo, S.K.; Becker, T.M.; Brown, M.E.; Denman, W.T.P.; Molyneux, P.; Hendrix, A.; Retherford, K.D.; Roth, L.; Alday, J. A New UV Spectral Feature on Europa: Confirmation of NaCl in Leading-Hemisphere Chaos Terrain. *arXiv* **2022**, arXiv:2201.01333. [CrossRef]

330. Bulat, A.; Yang, J.; Tzimiropoulos, G. To Learn Image Super-Resolution, Use a Gan to Learn How to Do Image Degradation First. In Proceedings of the European Conference on Computer Vision (ECCV) 2018, Munich, Germany, 8–14 September 2018; pp. 185–200.
331. Tang, Y.; Yan, P.; Yuan, Y.; Li, X. Single-Image Super-Resolution via Local Learning. *Int. J. Mach. Learn. Cybern.* **2011**, *2*, 15–23. [CrossRef]
332. Pickup, L.C. Machine Learning in Multi-Frame Image Super-Resolution. Ph.D. Thesis, University of Oxford, Oxford, UK, 2007.
333. Yang, J.; Fu, X.; Hu, Y.; Huang, Y.; Ding, X.; Paisley, J. PanNet: A Deep Network Architecture for Pan-Sharpening. In Proceedings of the 2017 IEEE Conference on Computer Vision and Pattern Recognition (CVPR), Honolulu, HI, USA, 21–26 July 2017; pp. 5449–5457.
334. Lee, J.; Lee, C. Fast and Efficient Panchromatic Sharpening. *IEEE Trans. Geosci. Remote Sens.* **2009**, *48*, 155–163.
335. Rahmani, S.; Strait, M.; Merkurjev, D.; Moeller, M.; Wittman, T. An Adaptive IHS Pan-Sharpening Method. *IEEE Geosci. Remote Sens. Lett.* **2010**, *7*, 746–750. [CrossRef]
336. Shah, V.P.; Younan, N.H.; King, R.L. An Efficient Pan-Sharpening Method via a Combined Adaptive PCA Approach and Contourlets. *IEEE Trans. Geosci. Remote Sens.* **2008**, *46*, 1323–1335. [CrossRef]
337. Morgan, G.A.; Putzig, N.E.; Perry, M.R.; Sizemore, H.G.; Bramson, A.M.; Petersen, E.I.; Bain, Z.M.; Baker, D.M.H.; Mastrogiuseppe, M.; Hoover, R.H. Availability of Subsurface Water-Ice Resources in the Northern Mid-Latitudes of Mars. *Nat. Astron.* **2021**, *5*, 230–236. [CrossRef]
338. Williams, J.; Day, M.; Chojnacki, M.; Rice, M. Scarp Orientation in Regions of Active Aeolian Erosion on Mars. *Icarus* **2020**, *335*, 113384. [CrossRef]
339. Williams, J.M.; Scuderi, L.A.; Newsom, H.E. Remote Sensing Computer Automation to Detect Erosional Scarps on Mars. In Proceedings of the Lunar and Planetary Science Conference 2021, Virtual conference, 15–19 March 2021; p. 1846.
340. Bishop, J.L.; Yeşilbaş, M.; Hinman, N.W.; Burton, Z.F.M.; Englert, P.A.J.; Toner, J.D.; McEwen, A.S.; Gulick, V.C.; Gibson, E.K.; Koeberl, C. Martian Subsurface Cryosalt Expansion and Collapse as Trigger for Landslides. *Sci. Adv.* **2021**, *7*, eabe4459. [CrossRef] [PubMed]
341. Banks, M.E.; McEwen, A.S.; Kargel, J.S.; Baker, V.R.; Strom, R.G.; Mellon, M.T.; Gulick, V.C.; Keszthelyi, L.; Herkenhoff, K.E.; Pelletier, J.D.; et al. High Resolution Imaging Science Experiment (HiRISE) Observations of Glacial and Periglacial Morphologies in the Circum-Argyre Planitia Highlands, Mars. *J. Geophys. Res. Planets* **2008**, *113*, E12015. [CrossRef]
342. Séjourné, A.; Costard, F.; Swirad, Z.M.; Łosiak, A.; Bouley, S.; Smith, I.; Balme, M.R.; Orgel, C.; Ramsdale, J.D.; Hauber, E.; et al. Grid Mapping the Northern Plains of Mars: Using Morphotype and Distribution of Ice-related Landforms to Understand Multiple Ice-rich Deposits in Utopia Planitia. *J. Geophys. Res. Planets* **2019**, *124*, 483–503. [CrossRef]
343. Orgel, C.; Hauber, E.; van Gasselt, S.; Reiss, D.; Johnsson, A.; Ramsdale, J.D.; Smith, I.; Swirad, Z.M.; Séjourné, A.; Wilson, J.T.; et al. Grid Mapping the Northern Plains of Mars: A New Overview of Recent Water-and Ice-related Landforms in Acidalia Planitia. *J. Geophys. Res. Planets* **2019**, *124*, 454–482. [CrossRef]
344. Levy, J.S.; Head, J.W.; Marchant, D.R. Lineated Valley Fill and Lobate Debris Apron Stratigraphy in Nilosyrtis Mensae, Mars: Evidence for Phases of Glacial Modification of the Dichotomy Boundary. *J. Geophys. Res. Planets* **2007**, *112*. [CrossRef]
345. Morgan, G.A.; Head, J.W., III; Marchant, D.R. Lineated Valley Fill (LVF) and Lobate Debris Aprons (LDA) in the Deuteronilus Mensae Northern Dichotomy Boundary Region, Mars: Constraints on the Extent, Age and Episodicity of Amazonian Glacial Events. *Icarus* **2009**, *202*, 22–38. [CrossRef]
346. Levy, J.; Head, J.W.; Marchant, D.R. Concentric Crater Fill in the Northern Mid-Latitudes of Mars: Formation Processes and Relationships to Similar Landforms of Glacial Origin. *Icarus* **2010**, *209*, 390–404. [CrossRef]
347. Levy, J.S.; Head, J.W.; Marchant, D.R. Concentric Crater Fill in Utopia Planitia: History and Interaction between Glacial "Brain Terrain" and Periglacial Mantle Processes. *Icarus* **2009**, *202*, 462–476. [CrossRef]
348. Levy, J.S.; Fassett, C.I.; Holt, J.W.; Parsons, R.; Cipolli, W.; Goudge, T.A.; Tebolt, M.; Kuentz, L.; Johnson, J.; Ishraque, F.; et al. Surface Boulder Banding Indicates Martian Debris-Covered Glaciers Formed over Multiple Glaciations. *Proc. Natl. Acad. Sci. USA* **2021**, *118*, e2015971118. [CrossRef]
349. Lu, Y.; Zhang, Z.; Shangguan, D.; Yang, J. Novel Machine Learning Method Integrating Ensemble Learning and Deep Learning for Mapping Debris-Covered Glaciers. *Remote Sens.* **2021**, *13*, 2595. [CrossRef]
350. Robson, B.A.; Bolch, T.; MacDonell, S.; Hölbling, D.; Rastner, P.; Schaffer, N. Automated Detection of Rock Glaciers Using Deep Learning and Object-Based Image Analysis. *Remote Sens. Environ.* **2020**, *250*, 112033. [CrossRef]
351. Xie, Z.; Haritashya, U.K.; Asari, V.K.; Young, B.W.; Bishop, M.P.; Kargel, J.S. GlacierNet: A Deep-Learning Approach for Debris-Covered Glacier Mapping. *IEEE Access* **2020**, *8*, 83495–83510. [CrossRef]
352. Ozdemir, A.; Polat, K. Deep Learning Applications for Hyperspectral Imaging: A Systematic Review. *J. Inst. Electron. Comput.* **2020**, *2*, 39–56. [CrossRef]
353. Li, S.; Song, W.; Fang, L.; Chen, Y.; Ghamisi, P.; Benediktsson, J.A. Deep Learning for Hyperspectral Image Classification: An Overview. *IEEE Trans. Geosci. Remote Sens.* **2019**, *57*, 6690–6709. [CrossRef]
354. Gewali, U.B.; Monteiro, S.T.; Saber, E. Machine Learning Based Hyperspectral Image Analysis: A Survey. *arXiv* **2018**, arXiv:1802.08701.
355. Audebert, N.; le Saux, B.; Lefèvre, S. Deep Learning for Classification of Hyperspectral Data: A Comparative Review. *IEEE Geosci. Remote Sens. Mag.* **2019**, *7*, 159–173. [CrossRef]

356. Signoroni, A.; Savardi, M.; Baronio, A.; Benini, S. Deep Learning Meets Hyperspectral Image Analysis: A Multidisciplinary Review. *J. Imaging* **2019**, *5*, 52. [CrossRef]
357. Bhatt, J.S.; Joshi, M.V. Deep Learning in Hyperspectral Unmixing: A Review. In Proceedings of the IGARSS 2020-2020 IEEE International Geoscience and Remote Sensing Symposium, Virtual, 26 September–2 October 2020; Institute of Electrical and Electronics Engineers (IEEE): Piscataway, NJ, USA, 2020; pp. 2189–2192.
358. Plebani, E.; Ehlmann, B.L.; Leask, E.K.; Fox, V.K.; Dundar, M.M. A Machine Learning Toolkit for CRISM Image Analysis. *Icarus* **2022**, 114849. [CrossRef]
359. Maheshwari, S.; Jain, R.C.; Jadon, R.S. A Review on Class Imbalance Problem: Analysis and Potential Solutions. *Int. J. Comput. Sci. Issues* **2017**, *14*, 43–51.
360. Abd Elrahman, S.M.; Abraham, A. A Review of Class Imbalance Problem. *J. Netw. Innov. Comput.* **2013**, *1*, 332–340.
361. Longadge, R.; Dongre, S. Class Imbalance Problem in Data Mining Review. *arXiv* **2013**, arXiv:1305.1707.
362. Galar, M.; Fernandez, A.; Barrenechea, E.; Bustince, H.; Herrera, F. A Review on Ensembles for the Class Imbalance Problem: Bagging-, Boosting-, and Hybrid-Based Approaches. *IEEE Trans. Syst. Man Cybern. Part C* **2011**, *42*, 463–484. [CrossRef]
363. Kotsiantis, S.; Kanellopoulos, D.; Pintelas, P. Handling Imbalanced Datasets: A Review. *GESTS Int. Trans. Comput. Sci. Eng.* **2006**, *30*, 25–36.
364. Satyasree, K.; Murthy, J. An Exhaustive Literature Review on Class Imbalance Problem. *Int. J. Emerg. Trends Technol. Comput. Sci.* **2013**, *2*, 109–118.
365. Ali, A.; Shamsuddin, S.M.; Ralescu, A.L. Classification with Class Imbalance Problem. *Int. J. Adv. Soft Comput. Appl.* **2013**, *5*.
366. Chawla, N.V.; Bowyer, K.W.; Hall, L.O.; Kegelmeyer, W.P. SMOTE: Synthetic Minority over-Sampling Technique. *J. Artif. Intell. Res.* **2002**, *16*, 321–357. [CrossRef]
367. Wang, L.; Chen, W.; Yang, W.; Bi, F.; Yu, F.R. A State-of-the-Art Review on Image Synthesis with Generative Adversarial Networks. *IEEE Access* **2020**, *8*, 63514–63537. [CrossRef]
368. Bowles, C.; Chen, L.; Guerrero, R.; Bentley, P.; Gunn, R.; Hammers, A.; Dickie, D.A.; Hernández, M.V.; Wardlaw, J.; Rueckert, D. GAN Augmentation: Augmenting Training Data Using Generative Adversarial Networks. *arXiv* **2018**, arXiv:1810.10863.
369. Bowles, C.; Gunn, R.; Hammers, A.; Rueckert, D. GANsfer Learning: Combining Labelled and Unlabelled Data for GAN Based Data Augmentation. *arXiv* **2018**, arXiv:1811.10669.
370. Han, W.; Feng, R.; Wang, L.; Chen, J. Supervised Generative Adversarial Network Based Sample Generation for Scene Classification. In Proceedings of the IGARSS 2019—2019 IEEE International Geoscience and Remote Sensing Symposium, Yokohama, Japan, 28 July–2 August 2019; pp. 3041–3044. [CrossRef]
371. Abady, L.; Barni, M.; Garzelli, A.; Tondi, B. GAN Generation of Synthetic Multispectral Satellite Images. In Proceedings of the Image and Signal Processing for Remote Sensing XXVI, Virtual, 21–25 September 2020; SPIE: Bellingham, WA, USA, 2020; Volume 11533, pp. 122–133.
372. Martinson, E.; Furlong, B.; Gillies, A. Training Rare Object Detection in Satellite Imagery with Synthetic GAN Images. In Proceedings of the 2021IEEE/CVF Conference on Computer Vision and Pattern Recognition (CVPR), Nashville, TN, USA, 20–25 June 2021; pp. 2769–2776.
373. Bosch, M.; Gifford, C.M.; Rodriguez, P.A. Super-Resolution for Overhead Imagery Using DenseNets and Adversarial Learning. In Proceedings of the 2018 IEEE/CVF Conference on Computer Vision and Pattern Recognition, Salt Lake City, UT, USA, 18–23 June 2018; pp. 1414–1422. [CrossRef]
374. Wang, C.; Zhang, Z.; Zhang, Y.; Tian, R.; Ding, M. GMSRI: A Texture-Based Martian Surface Rock Image Dataset. *Sensors* **2021**, *21*, 5410. [CrossRef]
375. McEwen, A.S.; Ojha, L.; Dundas, C.M.; Mattson, S.S.; Byrne, S.; Wray, J.J.; Cull, S.C.; Murchie, S.L.; Thomas, N.; Gulick, V.C. Seasonal Flows on Warm Martian Slopes. *Science* **2011**, *333*, 740–743. [CrossRef] [PubMed]
376. Howari, F.M.; Sharma, M.; Xavier, C.M.; Nazzal, Y.; Alaydaroos, F. Atmospheric, Geomorphological, and Compositional Analysis of Martian Asimov and Hale Craters: Implications for Recurring Slope Lineae. *Front. Astron. Space Sci.* **2022**, *8*, 781166. [CrossRef]
377. Wang, Y.; Di, K.; Xin, X.; Wan, W. Automatic Detection of Martian Dark Slope Streaks by Machine Learning Using HiRISE Images. *ISPRS J. Photogramm. Remote Sens.* **2017**, *129*, 12–20. [CrossRef]
378. Nagle-McNaughton, T.P. Synthetic Mars. Available online: https://doi.org/10.5281/zenodo.6338470 (accessed on 8 June 2022). [CrossRef]
379. Stepinski, T.F.; Mendenhall, M.P.; Molloy, I.; Bue, B.D.; Luo, W. *Automated Identification and Characterization of Landforms on Mars*; Elsevier: Amsterdam, The Netherlands, 2006.
380. Stepinski, T.F.; Ghosh, S.; Vilalta, R. Automatic Recognition of Landforms on Mars Using Terrain Segmentation and Classification. In Proceedings of the 9th International Conference on Discovery Science, Barcelona, Spain, 7–10 October 2006; Springer: Berlin/Heidelberg, Germany; pp. 255–266.
381. Tao, Y.; Muller, J.P.; Poole, W. Automated Localisation of Mars Rovers Using Co-Registered HiRISE-CTX-HRSC Orthorectified Images and Wide Baseline Navcam Orthorectified Mosaics. *Icarus* **2016**, *280*, 139–157. [CrossRef]
382. Li, S.; Xiong, L.; Tang, G.; Strobl, J. Deep Learning-Based Approach for Landform Classification from Integrated Data Sources of Digital Elevation Model and Imagery. *Geomorphology* **2020**, *354*, 107045. [CrossRef]
383. Sofia, G. Combining Geomorphometry, Feature Extraction Techniques and Earth-Surface Processes Research: The Way Forward. *Geomorphology* **2020**, *355*, 107055. [CrossRef]

384. Tarolli, P. High-Resolution Topography for Understanding Earth Surface Processes: Opportunities and Challenges. *Geomorphology* **2014**, *216*, 295–312. [CrossRef]
385. Eisank, C. An Object-Based Workflow for Integrating Spatial Scale and Semantics to Derive Landforms from Digital Elevation Models (DEMs). Ph.D. Thesis, University of Salzburg, Salzburg, Austria, April 2013.
386. D'Oleire-Oltmanns, S.; Eisank, C.; Drăgut, L.; Blaschke, T. An Object-Based Workflow to Extract Landforms at Multiple Scales from Two Distinct Data Types. *IEEE Geosci. Remote Sens. Lett.* **2013**, *10*, 947–951. [CrossRef]
387. Szypuła, B. Digital Elevation Models in Geomorphology. In *Hydro-Geomorphol. Models Trends*; Dericks, P.S., Ed.; IntechOpen: London, UK, 2017. [CrossRef]
388. Seijmonsbergen, A.C.; Hengl, T.; Anders, N.S. Chapter Ten—Semi-Automated Identification and Extraction of Geomorphological Features Using Digital Elevation Data. In *Geomorphological Mapping*; Smith, M.J., Paron, P., Griffiths, J.S.B.T.-D., Eds.; Elsevier: Amsterdam, The Netherlands, 2011; Volume 15, pp. 297–335. ISBN 0928-2025.
389. Anders, N.S.; Seijmonsbergen, A.C.; Bouten, W. Segmentation Optimization and Stratified Object-Based Analysis for Semi-Automated Geomorphological Mapping. *Remote Sens. Environ.* **2011**, *115*, 2976–2985. [CrossRef]
390. Drăguţ, L.; Blaschke, T. Automated Classification of Landform Elements Using Object-Based Image Analysis. *Geomorphology* **2006**, *81*, 330–344. [CrossRef]
391. Zhu, H.; Xu, Y.; Cheng, Y.; Liu, H.; Zhao, Y. Landform Classification Based on Optimal Texture Feature Extraction from DEM Data in Shandong Hilly Area, China. *Front. Earth Sci.* **2019**, *13*, 641–655. [CrossRef]
392. Nwacholundu, U.V.; Izuchukwu, I.J.; Ebele, E.J.; Onyedika, E.J.; Chinagorom, I.E. Generating and Analyzing Terrain Characteristics from Shuttle Radar Topographic Mission (SRTM), DEM. *World J. Adv. Res. Rev.* **2021**, *10*, 198–206. [CrossRef]
393. Shuanglin, L.; Fayuan, L. A Method of Automatic Topographic Recognition Based on Slope Spectrum. In *Geomorphometry for Geosciences*; Jasiewicz, J., Zwoliński, Z., Mitasova, H., Hengl, T., Eds.; Institute of Geoecology and Geoinformation, Adam Mickiewicz University in Poznań, International Society for Geomorphometry: Poznań, Poland, 2015; pp. 129–132.
394. Kharchenko, S. Automatic Recognition of Exogenic Landform Types on the Arctic Terrain Using Spectral Geomorphometric Variables (Example of the European Part of the Russia). *Int. Multidiscip. Sci. GeoConf. SGEM* **2019**, *19*, 785–791.
395. Abolt, C.J.; Young, M.H. High-Resolution Mapping of Spatial Heterogeneity in Ice Wedge Polygon Geomorphology near Prudhoe Bay, Alaska. *Sci. Data* **2020**, *7*, 87. [CrossRef] [PubMed]
396. Abolt, C.J.; Young, M.H.; Atchley, A.L.; Wilson, C.J. Brief Communication: Rapid Machine-Learning-Based Extraction and Measurement of Ice Wedge Polygons in High-Resolution Digital Elevation Models. *Cryosphere* **2019**, *13*, 237–245. [CrossRef]
397. Zhang, W.; Witharana, C.; Liljedahl, A.K.; Kanevskiy, M. Deep Convolutional Neural Networks for Automated Characterization of Arctic Ice-Wedge Polygons in Very High Spatial Resolution Aerial Imagery. *Remote Sens.* **2018**, *10*, 1487. [CrossRef]
398. Jorge, M.G.; Brennand, T.A. Semi-Automated Extraction of Longitudinal Subglacial Bedforms from Digital Terrain Models—Two New Methods. *Geomorphology* **2017**, *288*, 148–163. [CrossRef]
399. Saha, K.; Wells, N.A.; Munro-Stasiuk, M. An Object-Oriented Approach to Automated Landform Mapping: A Case Study of Drumlins. *Comput. Geosci.* **2011**, *37*, 1324–1336. [CrossRef]
400. Feizizadeh, B.; Kazemi Garajeh, M.; Blaschke, T.; Lakes, T. An Object Based Image Analysis Applied for Volcanic and Glacial Landforms Mapping in Sahand Mountain, Iran. *Catena* **2021**, *198*, 105073. [CrossRef]
401. Pedersen, G.B.M. Semi-Automatic Classification of Glaciovolcanic Landforms: An Object-Based Mapping Approach Based on Geomorphometry. *J. Volcanol. Geotherm. Res.* **2016**, *311*, 29–40. [CrossRef]
402. Martha, T.R.; Kerle, N.; Jetten, V.; van Westen, C.J.; Kumar, K.V. Characterising Spectral, Spatial and Morphometric Properties of Landslides for Semi-Automatic Detection Using Object-Oriented Methods. *Geomorphology* **2010**, *116*, 24–36. [CrossRef]
403. Mezaal, M.R.; Pradhan, B.; Sameen, M.I.; Shafri, H.Z.M.; Yusoff, Z.M. Optimized Neural Architecture for Automatic Landslide Detection from High-Resolution Airborne Laser Scanning Data. *Appl. Sci.* **2017**, *7*, 730. [CrossRef]
404. Pawłuszek, K.; Borkowski, A. Landslides Identification Using Airborne Laser Scanning Data Derived Topographic Terrain Attributes and Support Vector Machine Classification. In Proceedings of the International Archives of the Photogrammetry, Remote Sensing and Spatial Information Sciences, XXIII ISPRS Congress, Prague, Czech Republic, 12–19 July 2016; Volume 8.
405. Chudý, F.; Slámová, M.; Tomaštík, J.; Prokešová, R.; Mokroš, M. Identification of Micro-Scale Landforms of Landslides Using Precise Digital Elevation Models. *Geosciences* **2019**, *9*, 117. [CrossRef]
406. Martha, T.R.; Mohan Vamsee, A.; Tripathi, V.; Vinod Kumar, K. Detection of Coastal Landforms in a Deltaic Area Using a Multi-Scale Object-Based Classification Method. *Curr. Sci.* **2018**, *114*, 1338–1345. [CrossRef]
407. Scheip, C.M. Integrating Water-Classified Returns in DTM Generation to Increase Accuracy of Stream Delineations and Geomorphic Analyses. *Geomorphology* **2021**, *385*, 107722. [CrossRef]
408. Hughes, M.W.; Schmidt, J.; Almond, P.C. Automatic Landform Stratification and Environmental Correlation for Modelling Loess Landscapes in North Otago, South Island, New Zealand. *Geoderma* **2009**, *149*, 92–100. [CrossRef]
409. Kakavas, M.P.; Nikolakopoulos, K.G.; Zagana, E. Karst Features Detection and Mapping Using Airphotos, DSMs and GIS Techniques. In *Earth Resources and Environmental Remote Sensing/GIS Applications VI.*; SPIE: Bellingham, WA, USA, 2015; Volume 9644, pp. 174–183.
410. Kakavas, M.; Nikolakopoulos, K.G.; Kyriou, A.; Zagana, H. Assessment of Freely Available DSMs for Automatic Karst Feature Detection. *Arab. J. Geosci.* **2018**, *11*, 388. [CrossRef]

411. Mather, A.E.; Fyfe, R.M.; Clason, C.C.; Stokes, M.; Mills, S.; Barrows, T.T. Automated Mapping of Relict Patterned Ground: An Approach to Evaluate Morphologically Subdued Landforms Using Unmanned-Aerial-Vehicle and Structure-from-Motion Technologies. *Prog. Phys. Geogr. Earth Environ.* **2019**, *43*, 174–192. [CrossRef]
412. Del Val, M.; Iriarte, E.; Arriolabengoa, M.; Aranburu, A. An Automated Method to Extract Fluvial Terraces from LIDAR Based High Resolution Digital Elevation Models: The Oiartzun Valley, a Case Study in the Cantabrian Margin. *Quat. Int.* **2015**, *364*, 35–43. [CrossRef]
413. Thommeret, N.; Bailly, J.S.; Puech, C. Extraction of Thalweg Networks from DTMs: Application to Badlands. *Hydrol. Earth Syst. Sci.* **2010**, *14*, 1527–1536. [CrossRef]
414. Levy, J.S.; Fassett, C.I.; Rader, L.X.; King, I.R.; Chaffey, P.M.; Wagoner, C.M.; Hanlon, A.E.; Watters, J.L.; Kreslavsky, M.A.; Holt, J.W. Distribution and Characteristics of Boulder Halos at High Latitudes on Mars: Ground Ice and Surface Processes Drive Surface Reworking. *J. Geophys. Res. Planets* **2018**, *123*, 322–334. [CrossRef]
415. Rodriguez, J.A.P.; Fairén, A.G.; Tanaka, K.L.; Zarroca, M.; Linares, R.; Platz, T.; Komatsu, G.; Miyamoto, H.; Kargel, J.S.; Yan, J. Tsunami Waves Extensively Resurfaced the Shorelines of an Early Martian Ocean. *Sci. Rep.* **2016**, *6*, 25106. [CrossRef] [PubMed]
416. Moscardelli, L. Boulders of the Vastitas Borealis Formation: Potential Origin and Implications for an Ancient Martian Ocean. *GSA Today* **2014**, *24*, 4–10. [CrossRef]
417. Zimbelman, J.R. Transverse Aeolian Ridges on Mars: First Results from HiRISE Images. *Geomorphology* **2010**, *121*, 22–29. [CrossRef]
418. Burr, D.M.; Williams, R.M.E.; Wendell, K.D.; Chojnacki, M.; Emery, J.P. Inverted Fluvial Features in the Aeolis/Zephyria Plana Region, Mars: Formation Mechanism and Initial Paleodischarge Estimates. *J. Geophys. Res. Planets* **2010**, *115*. [CrossRef]
419. Weitz, C.M.; Milliken, R.E.; Grant, J.A.; McEwen, A.S.; Williams, R.M.E.; Bishop, J.L. Light-toned Strata and Inverted Channels Adjacent to Juventae and Ganges Chasmata, Mars. *Geophys. Res. Lett.* **2008**, *35*. [CrossRef]
420. Malin, M.C.; Edgett, K.S. Evidence for Persistent Flow and Aqueous Sedimentation on Early Mars. *Science* **2003**, *302*, 1931–1934. [CrossRef]
421. He, L.; Zhu, H.; Li, F.; Bai, H.; Cong, R.; Zhang, C.; Lin, C.; Liu, M.; Zhao, Y. Towards Fast and Accurate Real-World Depth Super-Resolution: Benchmark Dataset and Baseline. In Proceedings of the 2021 IEEE/CVF Conference on Computer Vision and Pattern Recognition (CVPR), Nashville, TN, USA, 20–25 June 2021; pp. 9229–9238.
422. Liang, Y.; Duan, N.; Gong, Y.; Wu, N.; Guo, F.; Qi, W.; Gong, M.; Shou, L.; Jiang, D.; Cao, G. Xglue: A New Benchmark Dataset for Cross-Lingual Pre-Training, Understanding and Generation. *arXiv* **2020**, arXiv:2004.01401.
423. Mu, N.; Gilmer, J. Mnist-c: A Robustness Benchmark for Computer Vision. *arXiv* **2019**, arXiv:1906.02337.
424. Deng, L. The Mnist Database of Handwritten Digit Images for Machine Learning Research [Best of the Web]. *IEEE Signal Process. Mag.* **2012**, *29*, 141–142. [CrossRef]
425. Luo, Z.; Branchaud-Charron, F.; Lemaire, C.; Konrad, J.; Li, S.; Mishra, A.; Achkar, A.; Eichel, J.; Jodoin, P.-M. MIO-TCD: A New Benchmark Dataset for Vehicle Classification and Localization. *IEEE Trans. Image Process.* **2018**, *27*, 5129–5141.
426. Xiao, H.; Rasul, K.; Vollgraf, R. Fashion-Mnist: A Novel Image Dataset for Benchmarking Machine Learning Algorithms. *arXiv* **2017**, arXiv:1708.07747.
427. Cohen, G.; Afshar, S.; Tapson, J.; van Schaik, A. EMNIST: Extending MNIST to Handwritten Letters. In Proceedings of the 2017 International Joint Conference on Neural Networks (IJCNN), Anchorage, AK, USA, 14–19 May 2017; Institute of Electrical and Electronics Engineers (IEEE): Piscataway, NJ, USA, 2017; pp. 2921–2926.
428. Wang, Y.; Jodoin, P.-M.; Porikli, F.; Konrad, J.; Benezeth, Y.; Ishwar, P. CDnet 2014: An Expanded Change Detection Benchmark Dataset. In Proceedings of the IEEE Conference on Computer Vision and Pattern Recognition Workshops, Columbus, OH, USA, 23–28 June 2014; pp. 387–394.
429. Zhou, W.; Newsam, S.; Li, C.; Shao, Z. PatternNet: A Benchmark Dataset for Performance Evaluation of Remote Sensing Image Retrieval. *ISPRS J. Photogramm. Remote Sens.* **2018**, *145*, 197–209. [CrossRef]
430. Uy, M.A.; Pham, Q.-H.; Hua, B.-S.; Nguyen, T.; Yeung, S.-K. Revisiting Point Cloud Classification: A New Benchmark Dataset and Classification Model on Real-World Data. In Proceedings of the IEEE/CVF International Conference on Computer Vision, Seoul, Korea, 27 October–2 November 2019; pp. 1588–1597.
431. Hwang, S.; Park, J.; Kim, N.; Choi, Y.; So Kweon, I. Multispectral Pedestrian Detection: Benchmark Dataset and Baseline. In Proceedings of the IEEE Conference on Computer Vision and Pattern Recognition, Boston, MA, USA, 7–12 June 2015; pp. 1037–1045.
432. Shi, B.; Wu, Z.; Mo, Z.; Duan, D.; Yeung, S.-K.; Tan, P. A Benchmark Dataset and Evaluation for Non-Lambertian and Uncalibrated Photometric Stereo. In Proceedings of the IEEE Conference on Computer Vision and Pattern Recognition, Las Vegas, NV, USA, 27–30 June 2016; pp. 3707–3716.
433. Guo, Y.; Zhang, L.; Hu, Y.; He, X.; Gao, J. Ms-Celeb-1m: A Dataset and Benchmark for Large-Scale Face Recognition. In Proceedings of the European Conference on Computer Vision, Amsterdam, The Netherlands, 11–14 October 2016; pp. 87–102.
434. Khan, N.Y.; McCane, B.; Wyvill, G. SIFT and SURF Performance Evaluation against Various Image Deformations on Benchmark Dataset. In Proceedings of the 2011 International Conference on Digital Image Computing: Techniques and Applications, Noosa, QLD, Australia, 18–21 July 2021; Institute of Electrical and Electronics Engineers (IEEE): Piscataway, NJ, USA, 2011; pp. 501–506.
435. Muller, M.; Bibi, A.; Giancola, S.; Alsubaihi, S.; Ghanem, B. Trackingnet: A Large-Scale Dataset and Benchmark for Object Tracking in the Wild. In Proceedings of the European Conference on Computer Vision (ECCV), Munich, Germany, 8–14 September 2018; pp. 300–317.

436. Li, C.; Guo, C.; Ren, W.; Cong, R.; Hou, J.; Kwong, S.; Tao, D. An Underwater Image Enhancement Benchmark Dataset and Beyond. *IEEE Trans. Image Process.* **2019**, *29*, 4376–4389. [CrossRef] [PubMed]
437. Goyette, N.; Jodoin, P.-M.; Porikli, F.; Konrad, J.; Ishwar, P. Changedetection. Net: A New Change Detection Benchmark Dataset. In Proceedings of the 2012 IEEE Computer Society Conference on Computer Vision and Pattern Recognition Workshops, Providence, RI, USA, 16–21 June 2012; Institute of Electrical and Electronics Engineers (IEEE): Piscataway, NJ, USA, 2012; pp. 1–8.
438. Oh, S.; Hoogs, A.; Perera, A.; Cuntoor, N.; Chen, C.-C.; Lee, J.T.; Mukherjee, S.; Aggarwal, J.K.; Lee, H.; Davis, L. A Large-Scale Benchmark Dataset for Event Recognition in Surveillance Video. In Proceedings of the CVPR 2011, Colorado Springs, CO, USA, 20–25 June 2011; Institute of Electrical and Electronics Engineers (IEEE): Piscataway, NJ, USA, 2011; pp. 3153–3160.
439. Perazzi, F.; Pont-Tuset, J.; McWilliams, B.; van Gool, L.; Gross, M.; Sorkine-Hornung, A. A Benchmark Dataset and Evaluation Methodology for Video Object Segmentation. In Proceedings of the IEEE Conference on Computer Vision and Pattern Recognition, Las Vegas, NV, USA, 27–30 June 2016; pp. 724–732.
440. Wang, W.Y. "Liar, Liar Pants on Fire": A New Benchmark Dataset for Fake News Detection. *arXiv* **2017**, arXiv:1705.00648.
441. Vacavant, A.; Chateau, T.; Wilhelm, A.; Lequievre, L. A Benchmark Dataset for Outdoor Foreground/Background Extraction. In Proceedings of the Asian Conference on Computer Vision, Daejeon, Korea, 5–9 November 2012; Springer: Berlin, Germany, 2012; pp. 291–300.
442. Wu, X.; Zhan, C.; Lai, Y.-K.; Cheng, M.-M.; Yang, J. Ip102: A Large-Scale Benchmark Dataset for Insect Pest Recognition. In Proceedings of the IEEE/CVF Conference on Computer Vision and Pattern Recognition, Long Beach, CA, USA, 15–20 June 2019; pp. 8787–8796.
443. LeCun, Y. The MNIST Database of Handwritten Digits. 1998. Available online: http://yann.lecun.com/exdb/mnist/ (accessed on 8 June 2022).
444. Harang, R.; Rudd, E.M. SOREL-20M: A Large Scale Benchmark Dataset for Malicious PE Detection. *preprint arXiv* **2020**, arXiv:2012.07634.
445. Sinka, M.P.; Corne, D.W. A Large Benchmark Dataset for Web Document Clustering. *Soft Comput. Syst. Des. Manag. Appl.* **2002**, *87*, 881–890.
446. Long, Y.; Xia, G.S.; Li, S.; Yang, W.; Yang, M.Y.; Zhu, X.X.; Zhang, L.; Li, D. On Creating Benchmark Dataset for Aerial Image Interpretation: Reviews, Guidances, and Million-AID. *IEEE J. Sel. Top. Appl. Earth Obs. Remote Sens.* **2021**, *14*, 4205–4230. [CrossRef]
447. Schmidt, D. Mars32k. Available online: https://dominikschmidt.xyz/mars32k/ (accessed on 8 June 2022).
448. Malin, M.C.; Bell, J.F.; Cantor, B.A.; Caplinger, M.A.; Calvin, W.M.; Clancy, R.T.; Edgett, K.S.; Edwards, L.; Haberle, R.M.; James, P.B. Context Camera Investigation on Board the Mars Reconnaissance Orbiter. *J. Geophys. Res. Planets* **2007**, *112*. [CrossRef]
449. Swan, R.M.; Atha, D.; Leopold, H.A.; Gildner, M.; Oij, S.; Chiu, C.; Ono, M. AI4MARS: A Dataset for Terrain-Aware Autonomous Driving on Mars. In Proceedings of the 2021 IEEE/CVF Conference on Computer Vision and Pattern Recognition Workshops (CVPRW), Nashville, TN, USA, 19–25 June 2021; pp. 1982–1991. [CrossRef]
450. Bickel, V.T.; Mandrake, L.; Doran, G. A Labeled Image Dataset for Deep Learning-Driven Rockfall Detection on the Moon and Mars. *Front. Remote Sens.* **2021**, *2*, 640034. [CrossRef]
451. Doran, G.; Dunkel, E.; Lu, S.; Wagstaff, K. Mars Orbital Image (HiRISE) Labeled Data Set Version 3.2. 2020. Available online: https://doi.org/10.5281/ZENODO.4002935 (accessed on 8 June 2022). [CrossRef]
452. Zhou, X.; Xie, X.; Xue, Y.; Xue, B.; Qin, K.; Dai, W. Bag of Geomorphological Words: A Framework for Integrating Terrain Features and Semantics to Support Landform Object Recognition from High-Resolution Digital Elevation Models. *ISPRS Int. J. Geo-Inf.* **2020**, *9*, 620. [CrossRef]
453. Schwenzer, S.P.; Woods, M.; Karachalios, S.; Phan, N.; Joudrier, L. Labelmars: Creating an Extremely Large Martian Image Dataset through Machine Learning. In Proceedings of the 50th Annual Lunar and Planetary Science Conference, The Woodlands, TX, USA, 18–22 March 2019; p. 1970.
454. Wallace, I.; Read, N.; Woods, M. Labelmars.Net: Driving Next-Generation Science Autonomy With Large High Quality Dataset Collection. In Proceedings of the 14th Symposium on Advanced SpaceTechnologies in Robotics and Automation, Leiden, the Netherlands, 20–22 June 2017.
455. Karachalios, S.; Woods, M.; Schwenzer, S.; Joudrier, L. Novelty or Anomaly Hunter: Towards Flight Ready Autonomous Science Using State of the Art Machine & Deep Learning. In Proceedings of the 15th Symposium on Advanced Space Technologies, Robotics and Automation, Noordwijk, The Netherlands, 27–28 May 2019.
456. Mandrake, L.; Braunegg, A.; Doran, G.; Horton, P.; Jeong, D.; Langert, E.; Lu, S.; Trockman, A.; Wagstaff, K.L. The Content-Based Object Summarization to Monitor Infrequent Change (COSMIC). Available online: https://www.zooniverse.org/projects/wkiri/cosmic/about/faq (accessed on 13 May 2022).
457. Doran, G.; Lu, S.; Liukis, M.; Mandrake, L.; Rebbapragada, U.; Wagstaff, K.L.; Young, J.; Langert, E.; Braunegg, A.; Horton, P.; et al. COSMIC: Content-Based Onboard Summarization to Monitor Infrequent Change. In Proceedings of the 2020 IEEE Aerospace Conference, Big Sky, MT, USA, 7–14 March 2020; pp. 1–12.
458. Aye, K.M.; Hansen, C.J.; Michaels, T.I.; Portyankina, A.; Schwamb, M. Planet Four. Available online: https://www.zooniverse.org/projects/mschwamb/planet-four/about/team (accessed on 13 May 2022).

459. Schwamb, M.E.; Aye, K.-M.; Portyankina, G.; Hansen, C.J.; Allen, C.; Allen, S.; Calef, F.J.; Duca, S.; McMaster, A.; Miller, G.R.M. Planet Four: Terrains—Discovery of Araneiforms Outside of the South Polar Layered Deposits. *Icarus* **2018**, *308*, 148–187. [CrossRef]
460. Portyankina, G.; Michaels, T.I.; Aye, K.-M.; Schwamb, M.E.; Hansen, C.J.; Lintott, C.J. Planet Four: Derived South Polar Martian Winds Interpreted Using Mesoscale Modeling. *Planet. Sci. J.* **2022**, *3*, 31. [CrossRef]
461. Kerber, L.; Schwamb, M.; Aye, K.M.; Portyankina, A.; Hansen, C.J. Planet Four: Ridges. Available online: https://www.zooniverse.org/projects/mschwamb/planet-four-ridges/about/research (accessed on 13 May 2022).
462. Khuller, A.R.; Kerber, L.; Schwamb, M.E.; Beer, S.; Nogal, F.E.; Perry, R.; Hood, W.; Aye, K.-M.; Portyankina, G.; Hansen, C.J. Irregular Polygonal Ridge Networks in Ancient Noachian Terrain on Mars. *Icarus* **2022**, *374*, 114833. [CrossRef]
463. Portyankina, G.; Hansen, C.J.; Aye, K.M. How Martian Araneiforms Get Their Shapes: Morphological Analysis and Diffusion-Limited Aggregation Model for Polar Surface Erosion. *Icarus* **2020**, *342*, 113217. [CrossRef]
464. Christensen, P.R.; Engle, E.; Anwar, S.; Dickenshied, S.; Noss, D.; Gorelick, N.; Weiss-Malik, M. JMARS-a Planetary GIS. In Proceedings of the AGU Fall Meeting Abstracts, San Francisco, CA, USA, 14–18 December 2009; Volume 2009, p. IN22A-06.